To the Graduate Council:

I am submitting herewith a thesis written by Mark Hale entitled "Field Emission Devices with Carbon Nanotube and Nanofiber Cathodes." I have examined the final electronic copy of this thesis for form and content and recommend that it be accepted in partial fulfillment of the requirements for the degree of Master of Science, with a major in Electrical Engineering.

Michael Simpson
Major Professor

We have read this thesis and recommend its acceptance:

Philip D. Rack

Benjamin J. Blalock

Accepted for the Council:

Anne Mayhew
Vice Provost and Dean of Graduate Studies

(Original signatures are on file with official student records)

Field Emission Devices with Carbon Nanotube and Nanofiber Cathodes

A Thesis Presented for the
Master of Science Degree
The University of Tennessee, Knoxville

Mark David Hale
May 2004

Dedication

To my parents

Jerry Brady Hale and Nancy Walker Hale

And to the memory of

James E. Poe

Acknowledgements

First and foremost I would like to thank Dr. Michael Simpson for supporting this research project, and for providing guidance and resources at Oak Ridge National Laboratory. I am also very grateful to Michael Crabtree, who provided financial support by establishing the Bodenheimer Fellowship that I received while pursuing my MS degree.

I would also like to thank Michael Guillorn for teaching me so much about microfabrication, and for excellent advice. Many thanks to Anatoli Melechko and Gyula Eres for assistance in growing carbon nanostructured materials. I also want to thank Pamela Fleming for helping me by metallizing many samples. In addition, I would like to thank Dale Hensley, Darrell Thomas, Steven Randolph, Richard Kasica, and Derek Austin. Lastly, I want to thank my family for always providing me with love and encouragement.

Abstract

This thesis presents research involving the fabrication and characterization of field emission devices utilizing carbon nanotubes and nanofibers as the field emission material. Carbon nanotube based gated cathodes were fabricated. These devices were tested under vacuum and were found to emit at low turn-on voltages. I-V data was obtained and was found to be in agreement with Fowler-Nordheim theory. Open top triodes were also fabricated and tested. The properties of these devices are discussed. A gate leakage current was measured on the carbon nanotube devices. This current was found to be caused by a carbon film deposited during the nanotube growth process. Experiments were also performed on the fabrication of carbon nanofiber based field emission devices. The results of these experiments are discussed.

Table of Contents

Chapter **Page**

1. Introduction 1
   - 1.1. The Current State of Vacuum Electronics 1
   - 1.2. Field Emission Devices 2
     - 1.2.1. Advantages of Field Emission Devices Over Traditional Vacuum Tubes 2
     - 1.2.2. Advantages of Field Emission Devices Over Solid-State Devices 3
   - 1.3. Materials for Microfabricated Cathodes in Field Emission Devices 3
     - 1.3.1. Field Emission Devices Using Carbon Nanostructured Materials ..4
   - 1.4. Thesis Objective 9

2. Carbon Nanostructured Materials 12
   - 2.1. Introduction to Carbon Nanostructured Materials 12
   - 2.2. Nanodiamond Films 12
   - 2.3. C_{60} Fullerenes 13
   - 2.4. Carbon Nanotubes 14
     - 2.4.1. Electrical Properties of Carbon Nanotubes 14
   - 2.5. Carbon Nanofibers 16

3. Theory of Device Operation 18
   - 3.1. Field Emission Theory 18
   - 3.2. Vacuum Requirements of Field Emission Devices 21
   - 3.3. Frequency Dependence of FE Device Operation 23
   - 3.4. Failure Mechanisms of Field Emission Devices 25

4. FE Device Fabrication 27
   - 4.1. Patterning and Deposition of Catalyst Material for Carbon Nanostructured Material Growth 27
     - 4.1.1. Photolithographic Equipment and Methods used for Device Fabrication 27
     - 4.1.2. Electron Gun Physical Vapor Deposition 28
   - 4.2. Deposition of the Dielectric Layer 29
   - 4.3. Chemical Vapor Deposition of Multiwall Carbon Nanotubes 30
   - 4.4. Plasma Enhanced Chemical Vapor Deposition of Carbon Nanofibers 31
   - 4.5. Chemical Mechanical Polishing 35
   - 4.6. Integration of Carbon Nanotubes with Microfabricated Structures 35

4.7. Integrating Carbon Nanofibers into Field Emission Devices 39
4.8. Fabrication of Carbon Nanotube Triode Devices 43

5. Experimental Procedures and Results.....45
5.1. Experimental Setup and Procedure 45
5.2. Experimental Results from Carbon Nanotube Gated Cathode FE Devices.....46
5.3. Experimental Results from Carbon Nanotube Triode FE Devices.....54
5.4. Drawbacks of the Electrical Characteristics of Carbon Nanotube Gated Cathodes and Triodes.....56

6. Conclusion 58
6.1. Summary and Analysis of Carbon Nanotube Field Emission Devices.....58
6.2. Summary and Analysis of Carbon Nanofiber Field Emission Devices.....58

References.....60

Vita.....65

List of Figures

Figure **Page**

1.1. A process flow diagram for microfabricated spindt-type field emitters 5
1.2. A carbon-nanoparticle FE device reported by Park *et al.* 6
1.3. Multi-walled carbon nanotube emitters for a FED prototype 8
1.4. A CNT triode fabricated using a MEMS process 10
1.5. A single VACNF field emission device 10

2.1. Diamond, graphite, C_{60}, and nanotube structures 13
2.2. Armchair, zigzag, and chiral orientations of nanotubes 15
2.3. Structure of carbon nanofibers with catalyst particles at their tips 17

3.1. Diagram of the potential energy at the surface of a metal with and without an applied field. The barrier height is lowered by the image charge 19
3.2. Plots of calculated emission current densities vs. V_g for: (a) fixed value of ϕ and varying values of β; (b) fixed value of β and varying values of ϕ 22
3.3. Normalized anode currents from molybdenum FEAs during exposure to oxygen at 4 different ambient pressures 24

4.1. 1 μm catalyst dot for nanofiber growth 29
4.2. TCVD grown carbon nanotubes in a gated cathode device 32
4.3. PECVD nanofiber growth system 33
4.4. Carbon nanofiber cathode 34
4.5. Carbon nanotube gated cathode device fabrication process 36
4.6. CVD result on an overetched gated cathode device 37
4.7. Etching of nanotubes in a 30 second oxygen plasma 38
4.8. Carbon nanofiber gated cathode fabrication process 40
4.9. Carbon nanofibers before and after oxide deposition and removal 41
4.10. Carbon nanofibers grown at 50 sccm C_2H_2 before and after oxide deposition and removal 42
4.11. Fabrication process for multiwall carbon nanotube triode devices 44

5.1. Test board for DC measurements 45
5.2. Switchbox for DC testing of FE devices 47
5.3. Measurement setup 48
5.4. A blowout curve performed prior to FE testing 48

5.5. FE I-V curve from an array of FE devices....50
5.6. Fowler-Nordheim plot of anode current....50
5.7. Field emission from an individual device....51
5.8. Field emission from an individual gated cathode device....52
5.9. Top: Emission before 40 minutes of constant voltage bias. Bottom: Emission after constant bias operation. 53
5.10. Carbon nanotube triode FE device....55
5.11. Carbon nanotube triode operation with constant 2nd gate voltage....55
5.12. Carbon nanotube triode operation with constant 1st gate voltage....56

Chapter 1

Introduction

1.1 The Current State of Vacuum Electronics

Thermionic vacuum tubes were once the dominant active component for electronic circuits. During this time, efforts were made to shrink the size and power consumption of these devices. However, in the late 1950s and early 1960s, vacuum tubes were quickly replaced by solid-state semiconductors. There were several reasons for this change in technology including the requirement of heating in order to emit electrons, thus decreasing the efficiency and limiting the miniaturization of the devices, and the space charge limitation of the maximum current density in vacuum tubes. Now only a few specialized applications remain in which vacuum tubes are favored over solid-state devices, such as in microwave power tubes and in cathode ray tubes[1.1].

Although vacuum electronic devices offer several advantages, to compete with solid-state devices they must be made smaller, more efficient, and produce higher current densities. Research performed on microfabricated vacuum electronic devices indicates that these devices could compete with and possibly replace solid-state devices in some applications.

1.2 Field Emission Devices

Vacuum microelectronic devices are promising for a variety of applications, including high power and high frequency amplifying devices; high temperature electronic devices; and electron beam sources for use in flat panel field emission displays (FED), e-beam lithography tools, and x-ray sources. Much research has been done on a class of vacuum microelectronic devices using field emission (high fields instead of thermal energy to initiate electron emission) for these applications.

The concept of field emitter arrays (arrays of microfabricated field emission sources) was first introduced by K.R. Shoulders[1,2]. These devices consist of microfabricated sharp tips on a cathode and commonly include an extraction electrode (gate). The gate is biased with a large positive voltage with respect to the cathode to initiate electron emission to an anode. The anode may be an external plate or a microfabricated electrode. These devices are operated at low pressures (less than 10^{-6} torr) and must be vacuum sealed for operation outside of a vacuum chamber. Gated field emitter arrays (FEAs) can be used for high frequency devices such as microwave power tubes (klystrons and traveling wave tubes) and also for on-chip devices that are similar to a field effect transistor[1,3].

1.2.1 Advantages of Field Emission Devices Over Traditional Vacuum Tubes

Field emission devices can be made much smaller than traditional thermionic vacuum tubes and require less power to operate because they do not require the cathode

to be heated to emit electrons. They can be turned on instantaneously, unlike thermionic vacuum tubes, which must be heated up before operation. FE devices may potentially operate at higher frequencies than traditional vacuum tubes as the separation between the electrodes can be made much smaller than in traditional vacuum tubes, thus decreasing the electron transit time[1.4].

1.2.2 Advantages of Field Emission Devices Over Solid-State Devices

Field emission devices have several advantages over solid-state devices including temperature independent operation, radiation-hardness, and frequency response. Solid-state devices experience carrier freeze out or runaway at temperature extremes, crystal structure damage by radiation resulting in degradation of performance[1.1], and an electron velocity three orders of magnitude lower than that in a vacuum[1.4].

1.3 Materials for Microfabricated Cathodes in Field Emission Devices

Several different materials have been reported for use as the electron emitting cathode in field emission devices. Microfabricated metal and silicon tips are common cathode materials. Spindt and coworkers fabricated metal field emitter arrays by evaporating metal through a shrinking aperture[1.5]. These were the first microfabricated field emitter arrays, and are known as Spindt-type emitters. The Spindt-type fabrication process produces cones of metal in the center of wells with gate electrodes encircling the top of the wells. A diagram for this process is shown below in Figure 1.1. Molybdenum,

titanium, niobium, zirconium and chromium have been used as the emitter for this process.

Silicon post emitters can be fabricated by etching posts in silicon and sharpening them in an oxidation process. An insulating layer of SiO_2 is grown around the post on top of which the gate electrode metal is deposited[1.3]. Unfortunately, silicon and metal field emitters are likely to form a surface oxide, which can degrade the performance of the device by hindering electron transport and by varying the work function during operation[1.6].

1.3.1 Field Emission Devices Using Carbon Nanostructured Materials

Recently, much research has been performed on integrating carbon nanostructured materials into microfabricated field emission devices. Thin film cathodes using carbon nanoparticle and diamond-like carbon films have been investigated, as well as tip or post emitters with a thin film coating. Park et al. successfully implemented a gated FE device utilizing a carbon-nanoparticle cathode grown by hot filament chemical vapor deposition (HFCVD) as shown in Figure 1.2[1.7]. This device displayed a turn on voltage (*Vth,* the gate voltage at which the device starts to emit electrons) of 45 volts. The current-voltage characteristics of this device agreed with the Fowler-Nordheim model of field emission.

Much research in vacuum nanoelectronics is now focused on carbon nanotubes (long cylindrically arranged graphitic sheets of carbon with diameters in the nanometer scale). Nanotubes are a promising material for field emission cathodes as they have a

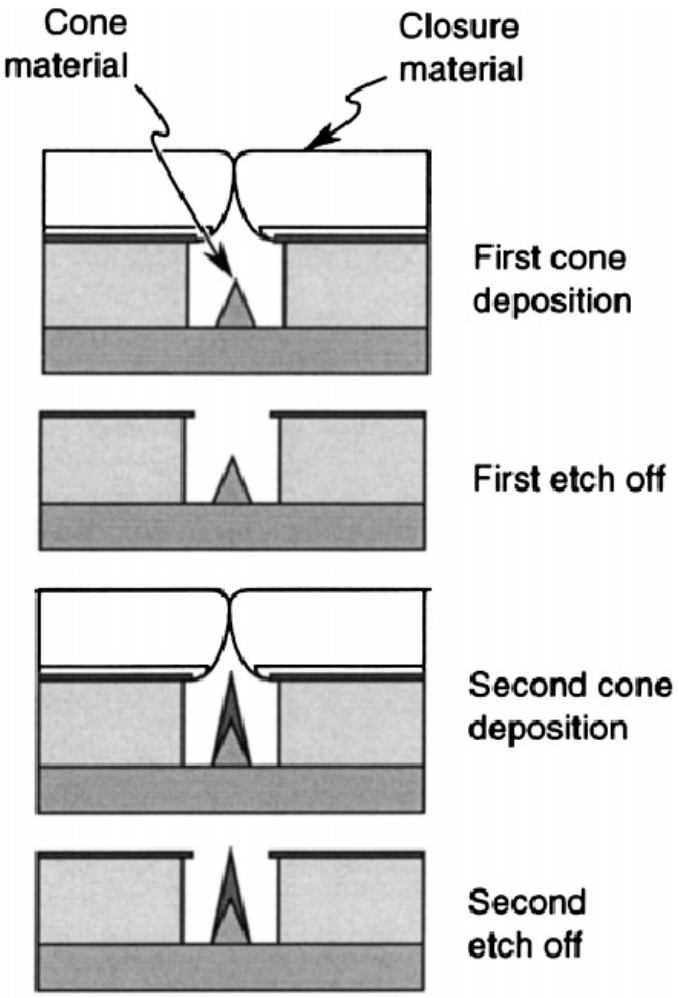


Figure 1.1: A process flow diagram for microfabricated spindt-type field emitters[1.3].

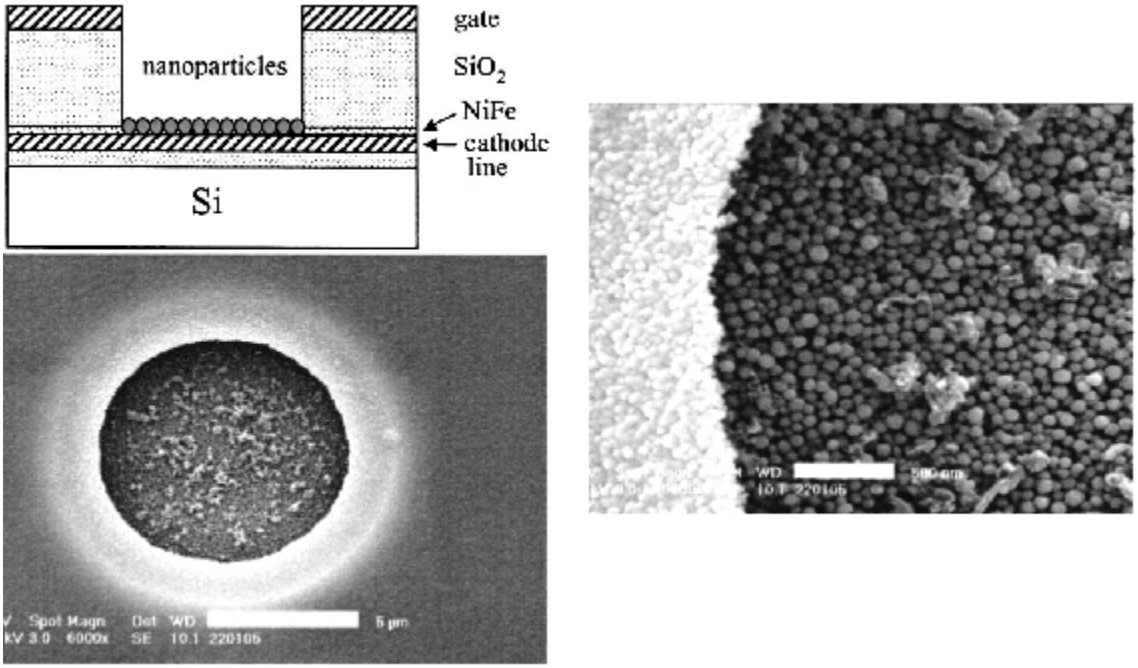


Figure 1.2: A carbon-nanoparticle FE device reported by Park *et al.*[1.7]

low threshold voltage for emission and have good environmental stability[1.8]. Another advantage of using nanotubes for field emission is their lack of a nonvolatile surface oxide[1.6].

Thin films of carbon nanotubes have been used as the cathode material in gated FEAs [1.4,1.6,1.8-13]. Xu and Brandes first demonstrated this by growing mats of multi-walled carbon nanotubes using thermal CVD[1.9]. A similar structure using CNTs grown by microwave plasma chemical vapor deposition (MPCVD) was reported by Cheng and coworkers[1.10]. The fabrication procedures used by Xu and Brandes and by Cheng et al involve a catalyst metal deposition for CNT growth inside a microfabricated well structure. A multiple electrode structure would be difficult to fabricate using this process, since the depth of the well increases with the number of electrodes. This problem can be defeated by depositing the catalyst material before the well is formed[1.11].

Hsu and Shaw demonstrated FEAs using HFCVD grown multiwall carbon nanotubes (MWNTs) as the cathode material on top of tall gated silicon posts[1.6]. Wang et al. fabricated a flat panel field emission display prototype using gated carbon nanotube cathodes as the pixel elements[1.12]. For the cathode material, MWNTs were synthesized in a dc arc system and used in forming a nanotube/polymer paste. This paste was deposited onto the cathode region of the device. SEM images of the MWNT emitter structures and the cathode surface are shown in Figure 1.3.

A carbon nanotube on-chip microtriode has been reported by C. Bower et al[1.4,1.13]. This device is constructed using a microelectromechanical systems (MEMS) fabrication process. A film of carbon nanotubes is grown on a hinged cathode, which is flipped on

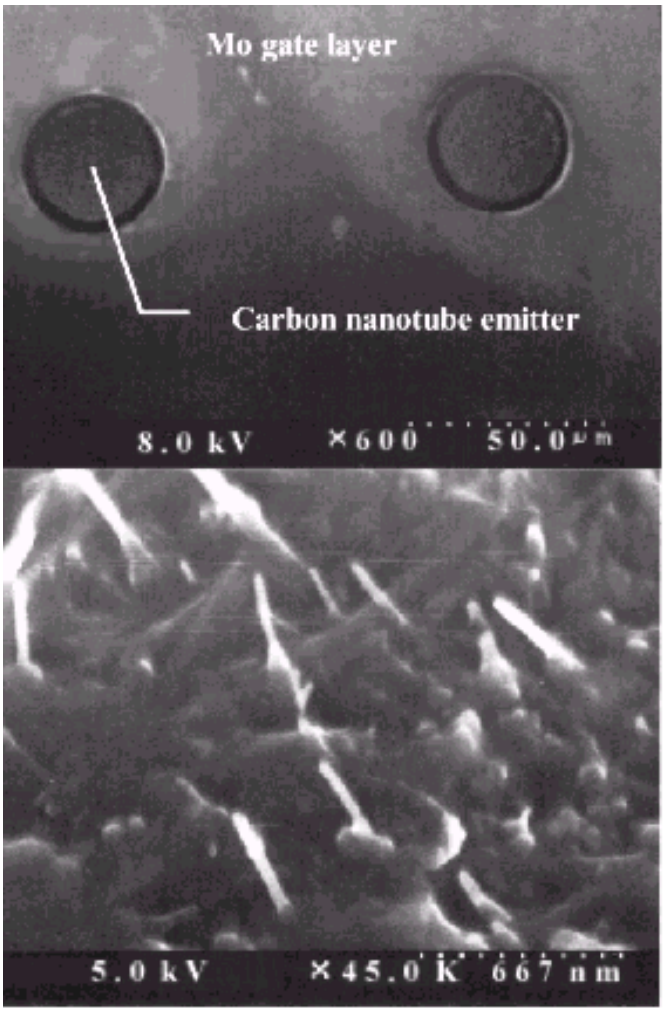


Figure 1.3: Multi-walled carbon nanotube emitters for a FED prototype[1.12].

its side and snapped into place to complete the device (Figure 1.4). Unfortunately, this MEMS fabrication process is not compatible with large-scale integrated circuit processes. Furthermore, the structure of this triode does not allow it to be easily sealed for use outside of a vacuum chamber.

FEDs employing a single carbon nanotube emitter have not reported, but a fabrication method for producing single vertically aligned carbon nanofibers (VACNF) in a microfabricated FE device has been demonstrated[1.14] (see Figure 1.5). The carbon nanofibers are composed of stacked graphene sheets that are rolled into a cone or cup shape, and they are grown by plasma enhanced chemical vapor deposition (PECVD). This structure with a single emission site can produce a more highly focused beam than a device with multiple emission sites, such as a nanotube film or multiple VACNF cathode. However, longer device lifetimes are possible in a field emission device with multiple emission sites as the device can still be operational if one emission site becomes damaged.

1.4 Thesis Objective

In this work I demonstrate a scalable process for making a vacuum sealable vertical triode device using nanostructured carbon for the emitter material. The objective of this work is to provide experimental data from and analysis of these devices in order to discuss their suitability for high frequency and high temperature applications. Chapter 2 discusses types of carbon nanostructured materials, and includes a description of the

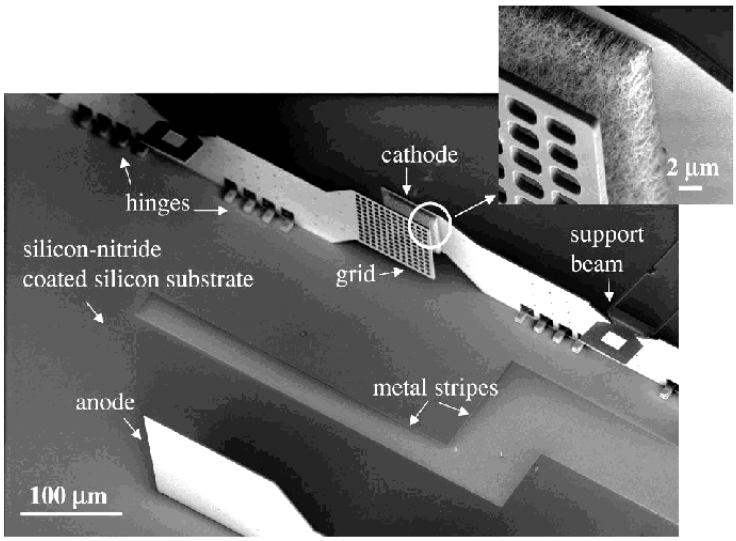


Figure 1.4: A CNT triode fabricated using a MEMS process[1.13].

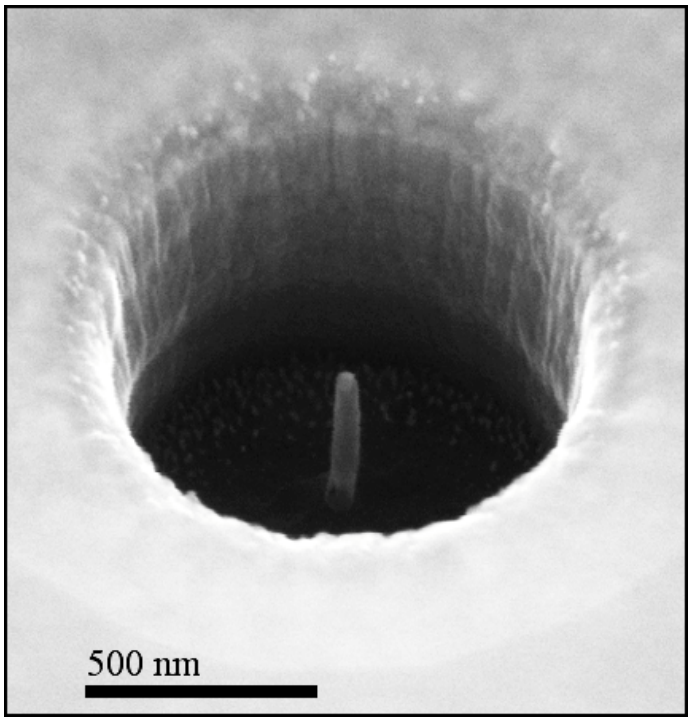


Figure 1.5: A single VACNF field emission device[1.14].

electronic and physical characteristics of carbon nanotubes and nanofibers. This chapter also includes discussion on methods for growing and characterizing carbon nanostructured materials.

Chapter 3 discusses the theoretical operation of the vacuum microelectonic device. It covers the Fowler-Nordheim current-voltage relationship, as well as the theoretical temperature dependence and high frequency operation of the device. This chapter concludes with a discussion of the possible failure mechanisms for the device.

Chapter 4 describes the fabrication process for making the devices. It includes a description of the microfabrication techniques and equipment used for making the devices, such as photolithography, thin film deposition and plasma etching. This chapter also discusses the issues involved with the integration of carbon nanostructured materials with these microfabrication techniques.

Chapter 5 begins with a description of the experimental setups and procedures used for measuring the characteristics of the field emission devices. The instrumentation used for characterizing the devices is described. DC current vs. voltage curves are presented both from gated cathode and triode devices. The performance of individual emitter cells within an array will be presented, as well as the performance of entire arrays of emitters. Data will also be presented for emitters that were tested after operating at a constant gate voltage.

Chapter 6 presents conclusions drawn from this work. Methods for improving the devices, such as a vacuum sealing procedure, will be discussed. Insights on the use of these devices for high frequency, high temperature, and other applications are provided.

Chapter 2

Carbon Nanostructured Materials

2.1 Introduction to Carbon Nanostructured Materials

Carbon-based materials have unique physical, chemical, mechanical, and electrical characteristics. For example, diamond has a high mechanical strength, excellent chemical inertness, high thermal conductance, and an exceptionally low friction coefficient[2.1]. Because of these unique properties of carbon materials, interest in synthesizing them on a nanometer scale has been recently escalating. Some of the many forms of carbon nanostructured materials include nanodiamond films, carbon onions, C_{60} fullerenes, carbon nanofibers, and carbon nanotubes.

2.2 Nanodiamond Films

Nanodiamond films are carbon films that have a low content of non-diamond phases, a uniform nanocrystallinity throughout the film, and a random grain orientation[2.2]. The high hardness of these films make them suitable for many mechanical applications, such as cantilivers for scanning force microscopy, high frequency micromechanical resonators, and wear-resistant coatings[2.3]. Nanodiamond films also have properties that make them desirable for field emission applications. These include good thermal and electrical conductivities, low electron affinity, and hardness to withstand ion

bombardment[2.4]. Nanodiamond films are commonly grown using hot filament chemical vapor deposition, but microwave plasma chemical vapor deposition and other CVD methods are also used[2.5].

2.3 C_{60} Fullerenes

C_{60} fullerenes are molecules of carbon formed in a truncated icosohedron shape resembling a sphere (see Figure 2.1 below). They were discovered in 1985 by Kroto et al[2.6]. There are many methods for producing C_{60} fullerenes, including laser sublimation of graphite in an inert gas atmosphere, resistive heating or arcing of graphite, combustion of hydrocarbons in sooting flames, and thermal decomposition of hydrocarbons[2.7].

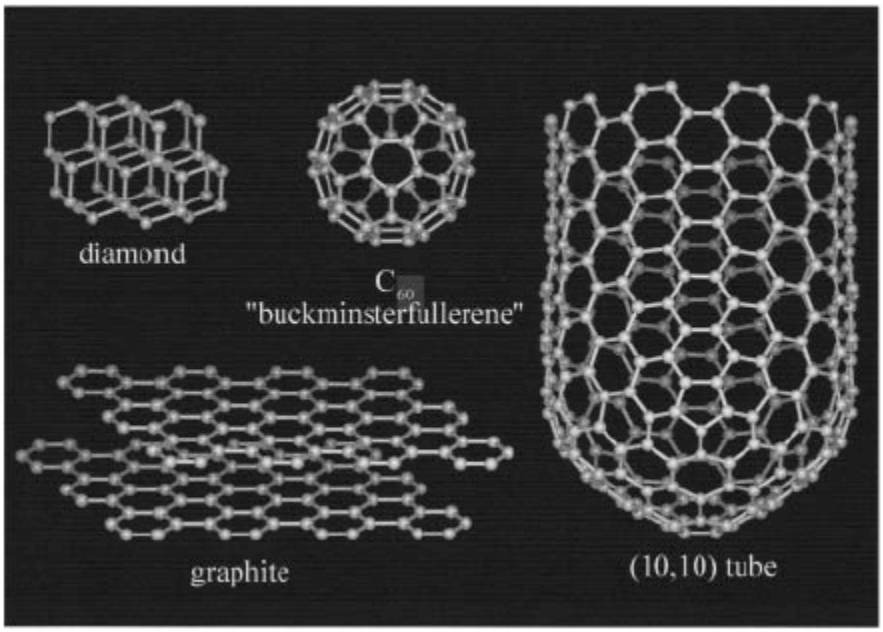


Figure 2.1: Diamond, graphite, C_{60}, and nanotube structures[2.7].

2.4 Carbon Nanotubes

The first reported observation of multi-walled carbon nanotubes was by Iijima in 1991, and single-walled nanotubes were soon after discovered experimentally by Iijima at the NEC Research Laboratory in Japan and by Bethune at the IBM Almaden Laboratory in California. Single-wall carbon nanotubes (SWNT) are a graphene sheet rolled into a hollow cylinder and capped at both ends by half of a fullerene molecule. Multi-walled nanotubes (MWNT) consist of a coaxial array of single-walled nanotubes seperated from one another by the interlayer distance of graphite, which is about .35 nm[2.8].

Graphene sheets are hexagonal networks of carbon atoms. The orientation of the hexagons on a nanotube depend on the way that the tube is rolled from a graphene sheet. Figure 2.2 below shows a schematic of a graphene sheet and illustrates how the chiral vector C_h and translation vector T are defined[2.9]. These vectors describe the orientation of the hexagons of carbon atoms on the nanotube surface. Models of the zigzag and and armchair tube orientations are shown in the figure. Tubes with zigzag or armchair orientation are highly symmetrical and achiral.

2.4.1 Electrical Properties of Carbon Nanotubes

Since the discovery of nanotubes, many observations have been made about their remarkable properties, such as their unusual electrical characteristics. Depending on its chirality and diameter, a nanotube may be either conducting or semiconducting. A SWNT is predicted to be metallic if the value of n-m from the chiral vector is equal to an

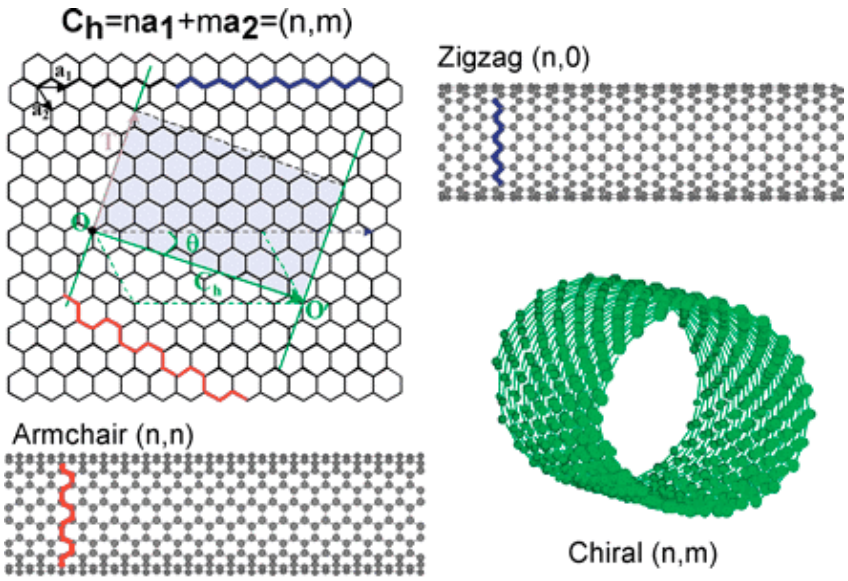


Figure 2.2: Armchair, zigzag, and chiral orientations of nanotubes[2.9].

integer divisible by three. If this value is not divisible by three, then the SWNT is predicted to be semiconducting[2.9]. These predictions can be made if the nanotube has a large enough diameter for the hybridization effects of neighboring π bonds to be ignored. For small diameter nanotubes, the hybridization orbitals can affect the electronic behavior of SWNTs[2.9].

In addition to conductors and semiconductors, carbon nanotubes can be used as field emitters. Electric fields are enhanced at their sharp tips and small diameters to allow emission of electrons at low voltages. Thin films of carbon nanotubes have been reported to emit electrons at voltages as low as1.5V/μm and to yield current densities greater than 10mA cm^{-2} [2.10]. The emission performance of SWNT films degrade significantly with time, but this degradation is much less with films of multiwalled nanotubes[2.10].

2.5 Carbon Nanofibers

Apart from having small grain sizes compared to their circumferences, carbon nanofibers are similar in structure to carbon nanotubes (which are single crystalline grains)[2.11]. This disordered structure is represented below in Figure 2.3. The carbon nanofibers in Figure 2.3 were grown using a plasma enhanced chemical vapor deposition method. This PECVD method for growing vertically aligned carbon nanofibers (VACNFs) on patterned Ni catalyst dots was first reported by Ren et al[2.12].

Figure 2.3 shows that the carbon nanofibers have Ni dots at their tips. The initial Ni catalyst particles are large compared to these dots. The catalyst particles are broken up into small droplets during a pre-growth plasma etch. These droplets initiate catalytic growth when acetylene is introduced into the dc plasma[2.11].

Possible applications for VACNFs include field emission arrays[2.13], scanning-probe microscopy, electrochemical probes for intracellular characterization[2.14], and templates for the construction of nanofluidic devices[2.15]. An advantage of carbon nanofibers over nanotubes for field emission applications is the superior ability of the nanofiber growth process to control the placement and orientation of the fibers.

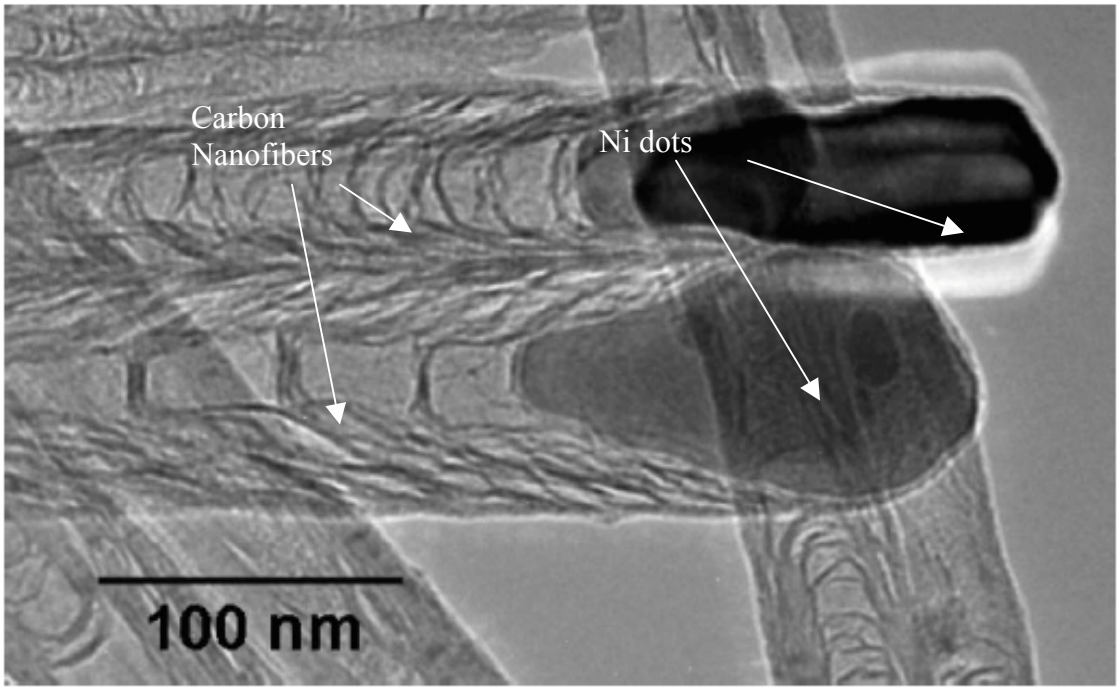


Figure 2.3: Structure of carbon nanofibers with catalyst particles at their tips[2.11].

Chapter 3

Theory of Device Operation

3.1 Field Emission Theory

Field emission is the tunneling of electrons through a narrow potential barrier at the surface of a solid. Applied fields on the order of 10^7 V/cm can bend the potential energy function steeply to form a narrow potential energy barrier at the surface. The finite width of this barrier allows electrons at the Fermi energy level (E_F) to tunnel through and escape into vacuum. Figure 3.1 below shows a diagram of the electron potential energy at the surface of a metal with and without an applied field.

The dashed line in Figure 3.1 shows the shape of the potential energy barrier with no applied electric field. The barrier height is the work function ϕ of the metal, which is the energy required for an electron to be moved from the Fermi level to the vacuum level. The solid line in Figure 3.1 represents the shape of the potential energy barrier with an external electric field applied. The field causes the potential energy barrier to be triangular shaped. As seen in Figure 3.1, the barrier is lowered and rounded. This reduction of the barrier height is caused by charge outside of the surface that induces charge at the surface of the metal. This charge is known as image charge.

The energy required for an electron to be moved from the Fermi level to the

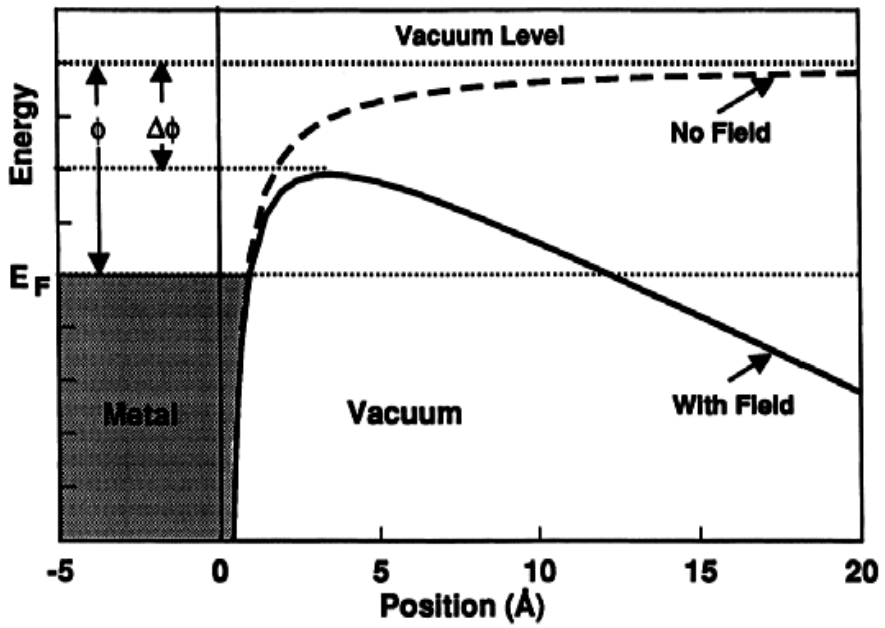


Figure 3.1: Diagram of the potential energy[3.1] at the surface of a metal with and without an applied field. The barrier height is lowered by the image charge.

vacuum level is now $\Delta\phi$, given by[3.1]

$$\Delta\phi = \left(\frac{eE}{4\pi\varepsilon_0}\right)^{1/2} \tag{3-1}$$

where e is the electron charge, E is the applied field, and ε_0 is the permittivity of vacuum.

An expression for the tunneling current density can be derived by integrating a function describing the probability of an electron with a given energy of tunneling from the metal into the vacuum multiplied by a function describing the electron supply in the available range of electron energies. This results in the Fowler-Nordheim equation[3.1]

$$J = \frac{e^3 E^2}{8\pi h \phi t^2(y)} \exp\left[\frac{-8\pi(2m)^{1/2}\phi^{3/2}}{3heE} v(y)\right] \tag{3-2}$$

where y=Δϕ/ϕ, h is Planck's constant, *m* is the electron mass, and t(y) and v(y) are the Nordheim elliptic functions. The value for t^2(y) is approximately 1.1, and the value for *v*(y) is approximately .95-y^2 [3.1]. *J* is in units of A/cm^2, *E* is in units of V/cm and ϕ is in units of eV. Using these values in equation (3-2) gives equation (3-3) below[3.1]. A linear relationship with a slope proportional to $\phi^{3/2}$ results when log(J/E^2) is plotted vs. 1/*E*:

$$J = 1.42 \times 10^{-6} \frac{E^2}{\phi} \exp\left(\frac{10.4}{\phi^{1/2}}\right) \exp\left(\frac{-6.44 \times 10^7 \phi^{3/2}}{E}\right) \tag{3-3}$$

Equation (3-3) applies for a temperature of 0°K. There is negligible error involved in the use of this equation at moderate temperatures (300°K). However, for high temperatures at which thermionic emission normally begins, the current becomes dependent on temperature and includes both thermionic and field emission current[3.2,3.3].

The electric field in microfabricated field emitters is enhanced by the sharp tips of the emitters. When a gate voltage V_g is applied, the electric field *E* at the tip is given by[3.1]

$$E = \beta \times V_g \tag{3-4}$$

where β is the field enhancement factor in units of cm^{-1}. The emission current is largely dependent on the field enhancement factor β and the work function ϕ. The value of the work function depends on the electronic properties of the emitter surface. The field enhancement factor depends on the geometry of the FE device. The parameters that have the strongest effect on β are the emitter tip radius of curvature and the diameter of the gate aperture, with β increasing as these two parameters are decreased. Figure 3.2 (a)

shows plots of the calculated emission current density J vs. V_g with a fixed work function ϕ=4eV and with β varying from 3 X 10^5 to 6 X 10^5 cm^{-1}. Figure 3.2 (b) shows the calculated J vs. V_g with a fixed field enhancement factor β=4 X 10^5 cm^{-1} and ϕ varying from 2 to 5 eV. These plots show that the emission current increases as β increases and ϕ decreases and that the turn-on voltages decrease as β is increased and ϕ decreases.

The work function of MWNTs has been estimated by Chen et al.[3.4] and Ago et al.[3.5] to be 5.7 eV and 4.3 eV, respectively. The discrepancy (and the lack of explanation for it) indicates that it is difficult to accurately measure the work function of carbon nanotubes under present experimental conditions. It is also difficult to determine the field enhancement factor of a MWNT FE device with multiple emission sites, but it is known that it will be high due to the small tip radii of the nanotubes.

3.2 Vacuum Requirements of Field Emission Devices

Low pressures are needed to minimize the effects of gas molecules in the chamber on the emitter performance. Adsorption of gas molecules on the emitter tip occurs more frequently at higher pressures. This adsorption causes a change in the work function of the tip. The tip surface can be cleaned of adsorbates by high emission Joule heating[3.6], but adsorption will reoccur if the tip cools. Impact ionization also occurs more frequently at higher pressures and can result in the bombardment of the cathode by ions.
FE devices operate best in ultra-high vacuum conditions (1 X 10^{-8} Torr or less), but they are sometimes operated at higher pressures in gases such as O_2 and water vapor.

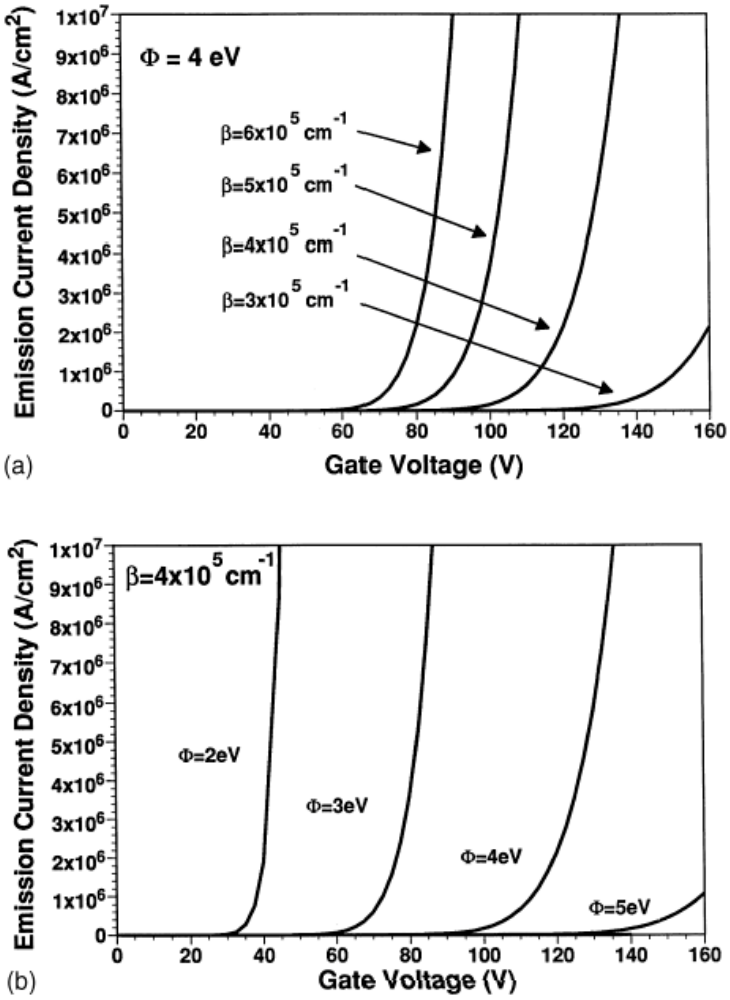


Figure 3.2: Plots of calculated emission current densities vs. V_g for: (a) fixed value of ϕ and varying values of β; (b) fixed value of β and varying values of ϕ[3.1].

Figure 3.3 shows the effect of exposing molybdenum Spindt-type FEAs to oxygen at four different pressures as reported by Chalamala, Wallace, and Gnade[3.7]. The four different curves were taken at different ambient pressures ranging from 2 X 10^{-10} to 1 X 10^{-6} Torr, and are normalized to the anode current that was observed before the oxygen was introduced. The introduction of oxygen caused a reduction in the anode current. It was observed that the magnitude of the emission current returned to the original value when the pressure was decreased back to 2 X 10^{-10}.

3.3 Frequency Dependence of FE Device Operation

The high frequency operation of a FE device is limited by the transconductance and capacitance of the device. The cutoff frequency of the device is given as[3.8]

$$f_t = g_m / 2\pi C_g \tag{3-5}$$

where g_m is the transconductance of the device, or the change in anode current caused by a change in gate voltage ($\Delta Ia/\Delta Vg$), and C_g is the capacitance of the device. Equation 3-5 shows that high frequency operation requires a high transconductance and low capacitance.

The capacitance of the device depends on the overlapping area between the cathode and gate electrodes, the distance between the electrodes, and the dielectric constant of the insulating material between the electrodes. The capacitance of the device can be minimized by decreasing the area of the electrodes, increasing the distance

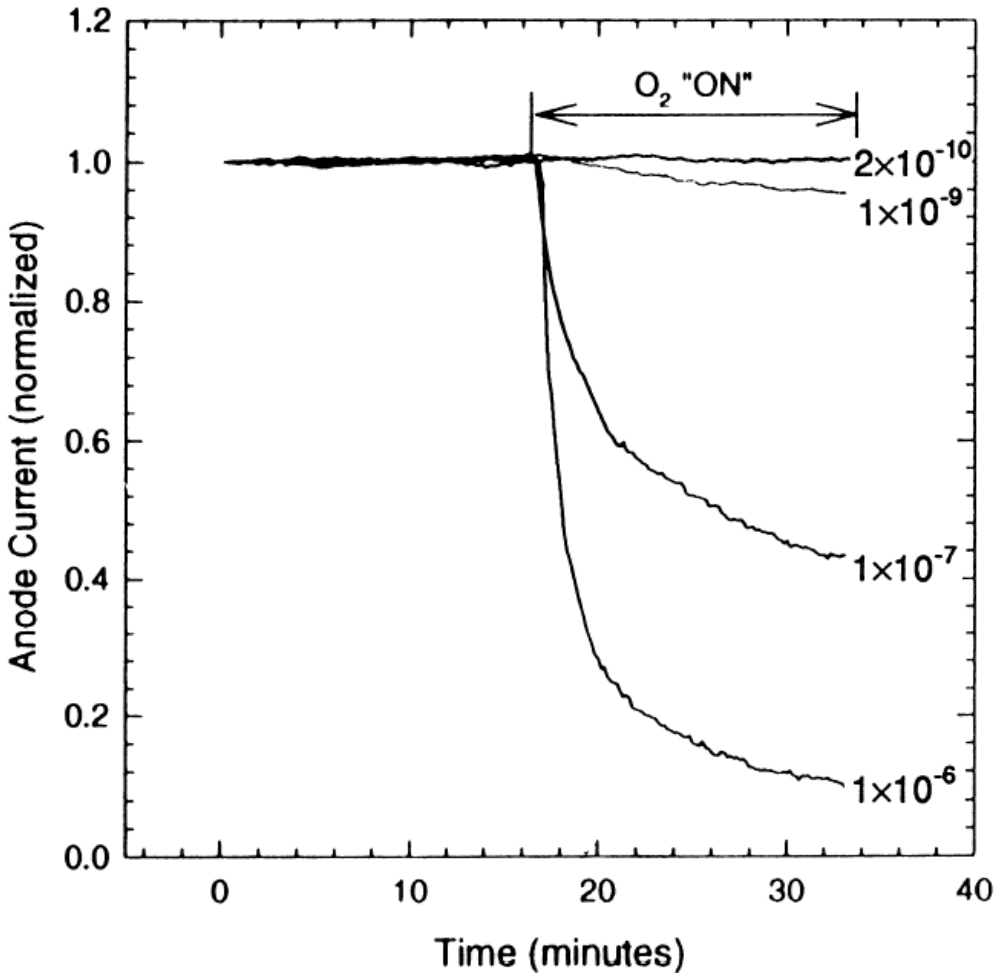


Figure 3.3: Normalized anode currents from molybdenum FEAs during exposure to oxygen at 4 different ambient pressures[3.7].

between the electrodes, and using an insulating material with a low dielectric constant.

The transconductance of a FE array depends on parameters that affect the emission current from the tips, such as the tip shape, the gate aperture diameter, and the work function of the tip[3.8]. The transconductance increases as the amount of current per tip in the array increases, and is proportional to the number of tips in an array. One way of improving the g_m is to increase the field enhancement factor[3.9]. β can be increased by decreasing the gate apertures of the field emission devices, but the decrease in emission area involved with this method should be considered. Increasing the packing density of emitters can also improve the transconductance.

3.4 Failure Mechanisms of Field Emission Devices

Operating FE devices at high emission currents can result in degradation or failure of the devices. Dean, Burgin, and Chalamala report that localized heating can occur in single walled nanotubes emitting at high current densities, which results in thermally assisted field evaporation of carbon atoms from the nanotube cap[3.10]. This field evaporation can change the field emission properties of nanotubes by shortening the length of the nanotubes and restructuring the tips. Unlike metal field emitters, the field evaporation of carbon atoms occurs without arcing, which would destroy the emitter. Gradual degradation of nanotube emitters can also be caused by ion bombardment from the gas phase or by selective oxidation[3.11]. Abrupt failure of nanotube FE devices can be caused by arcing or mechanical failure. Arcing can be caused by a high field emission

current, anode outgassing, or local evaporation of the cathode material that creates a short between the electrodes. Mechanical failure of nanotube emitters can occur when the nanotube is under high tensile stress caused by a high electric field[3.11].

Chapter 4

FE Device Fabrication

4.1 Patterning and Deposition of Catalyst Material for Carbon Nanostructured Material Growth

In order to grow carbon nanotubes and nanofibers, a catalyst material must first be patterned onto the surface of the substrate[4.1,4.2]. Four inch 1-10 Ω·cm Si n-type wafers were used as the substrate of the devices. The catalyst pattern was defined using photolithography (refer to section 4.1.1), and catalyst metal was deposited using an electron gun physical vapor deposition process described in section 4.1.2. The catalyst metal on unpatterned areas of the wafer was lifted off in acetone.

4.1.1 Photolithographic Equipment and Methods used for Device Fabrication

For this work, initial photolithography was performed using an HTG contact aligner. Shipley 1813 and 1818 photoresists and MF CD26 developer were used for processing wafers exposed with this tool. Before patterning catalyst sites, alignment marks were patterned in photoresist and reactive ion etching (RIE) was used to etch the marks into the wafer. For devices processed with the contact aligner, the catalyst pattern consisted of 10 μm squares. This relatively large catalyst site was chosen as it is difficult to achieve alignment precision much less than ten microns using this contact aligner. The

large catalyst site helped to ensure that the 4 μm gate apertures would be aligned over the catalyst in a later fabrication step.

For a clean liftoff pattern transfer, a negative step profile was desired in the unexposed resist. This would prevent metal from being deposited onto the sidewall of the resist. To achieve this, the catalyst pattern was exposed onto positive photoresist using a negative tone brightfield mask. The exposed resist was treated in an image reversal process using a Yield Engineering Systems image reversal oven before flood exposing and developing the wafer.

A GCA Autostep 200 5x reduction step and repeat system was used for photolithography. This tool is capable of achieving alignment precision of better than 125 nm. Catalyst sites for devices processed with this tool consisted of 1 μm dot. A catalyst dot after e-beam deposition and liftoff is shown below in Figure 4.1.

4.1.2 Electron Gun Physical Vapor Deposition

Thin films of metal are needed for the catalyst and gate metal of the devices. An electron gun physical vapor deposition (PVD) tool was used for these purposes. For nanotube growth, a dual layer of 10 nm Al and 1 nm Fe was used as the catalyst material. The carbon nanofiber catalyst consists of 10 nm Ti and 10 nm Ni. The deposition of these metals was done at pressures less than 1 E-6 Torr. E-beam PVD was also used for the deposition of the gate metal of the device, which consisted of 50 nm Mo.

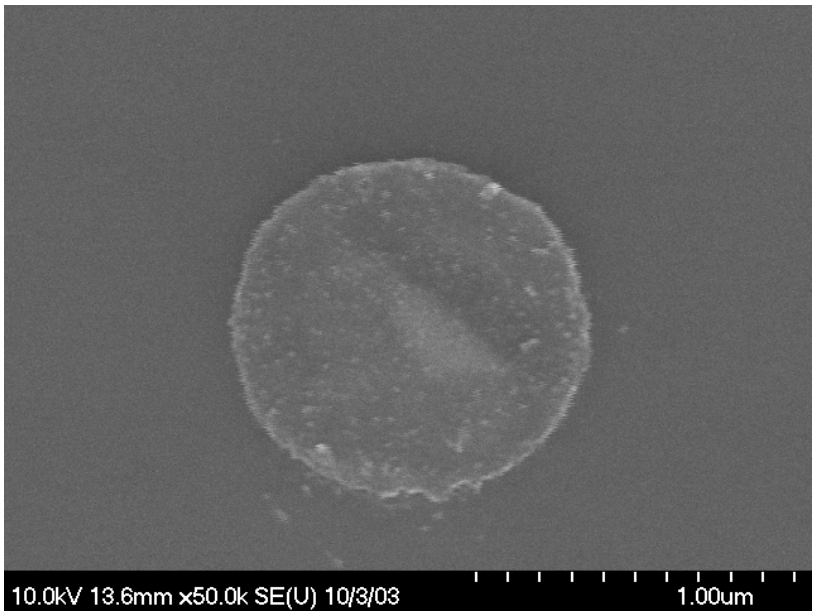


Figure 4.1: 1 μm catalyst dot for nanofiber growth.

4.2 Deposition of the Dielectric Layer

To electrically isolate the gate from the substrate of the FED, a thin film of silicon dioxide was deposited using a Trion Technologies Orion rf plasma enhanced chemical vapor deposition system (PECVD). The deposition temperature was 400°C, and the pressure was 1 Torr. Silane and nitrous oxide flow rates were 140 sccm, while the rf power was 100W. Under these conditions, silicon oxide was deposited at a rate of 160 nm/min with an index of refraction of 1.46. The deposition conditions were changed on some occasions to counter changes in the characteristics of the oxide from the tool. The thickness uniformity of the oxide was usually within 10 % across a four inch wafer,

excepting the areas within 10 mm of the edge, where the deposition rate dropped off significantly.

The PECVD oxide was required to withstand high electric fields without breaking down and was required to survive the high temperature CVD process without any significant degradations in quality. To test the quality of the oxide, a 1 μm layer was deposited on a silicon wafer. Molybdenum electrodes were deposited onto the oxide. A voltage sweep from 0 to 1 kV was applied to the electrodes. The average breakdown voltage of the tested samples was 848 V. Several samples were heated at 900°C for 1.5 hours before testing, which reduced the average breakdown voltage to 742 V. The PECVD oxide had no significant leakage current before breakdown, and the oxide did not break down at the potential applied during FE testing (usually less than 100 V/ μm).

4.3 Chemical Vapor Deposition of Multiwall Carbon Nanotubes

The method used for growth of multiwall carbon nanotubes in these FEDs was Thermal Chemical Vapor Deposition (TCVD). This growth is the last step in the fabrication of the nanotube FE devices. Before this growth, a 4 μm gate aperture is defined using photolithography. An RIE process is used to etch the aperture pattern through the gate metal and oxide to uncover the catalyst metal. To begin the TCVD growth process, the sample is placed in a hot wall quartz tube reactor and heated at approximately 750 Torr while 500 sccm Ar and 100 sccm H_2 are flowed. A C_2H_2 flow is

introduced when the sample reaches the final temperature, which ranged from 650 to 900°C for growth experiments. The Al in the catalyst metal is heated beyond its melting point, which aids in the formation of nanoparticles in the Fe film. The C_2H_2 reacts with the catalyst particles to initiate nanotube growth. Figure 4.2 shows carbon nanotubes grown using this process. Further discussion of the fabrication process of the nanotube devices can be found in section 4.6.

4.4 Plasma Enhanced Chemical Vapor Deposition of Carbon Nanofibers

Nanofiber growth is performed immediately after the catalyst deposition in FE devices with nanofibers. The PECVD chamber consists of a glass bell-jar which is evacuated by a roughing pump (see Figure 4.3). The cathode is resistively heated and this temperature is carefully controlled. The anode consists of stainless steel rods.

Samples are placed on the cathode for nanofiber growth. Growth occurs in a DC plasma with the cathode heated to 700°C. As the sample is heated, 80 sccm NH_3 is flowed at 3 Torr. Acetylene (C_2H_2) is flowed at a rate of 20 sccm for 10 seconds after the temperature reaches 700°C. After 10 seconds, the PECVD power supply is turned on to create a plasma between the anode and cathode. The power supply is set to source 400 mA, and the anode voltage is usually between 500 and 600 volts. During the first minute of growth, the acetylene flow rate is manually ramped from 20 to 56 sccm. The total growth time is 3 minutes to produce nanofibers that are 600-800 nm tall. Figure 4.4 shows nanofibers grown on a catalyst dot using this process.

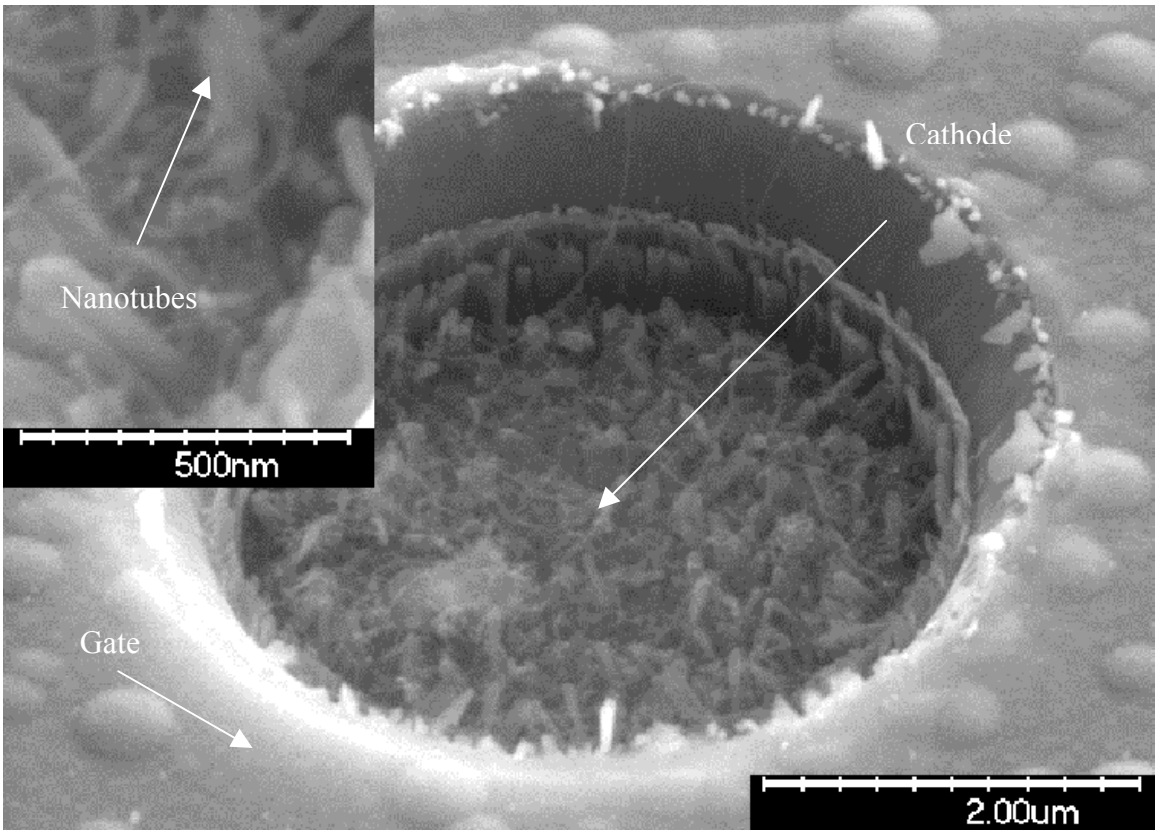


Figure 4.2: TCVD grown carbon nanotubes in a gated cathode device.

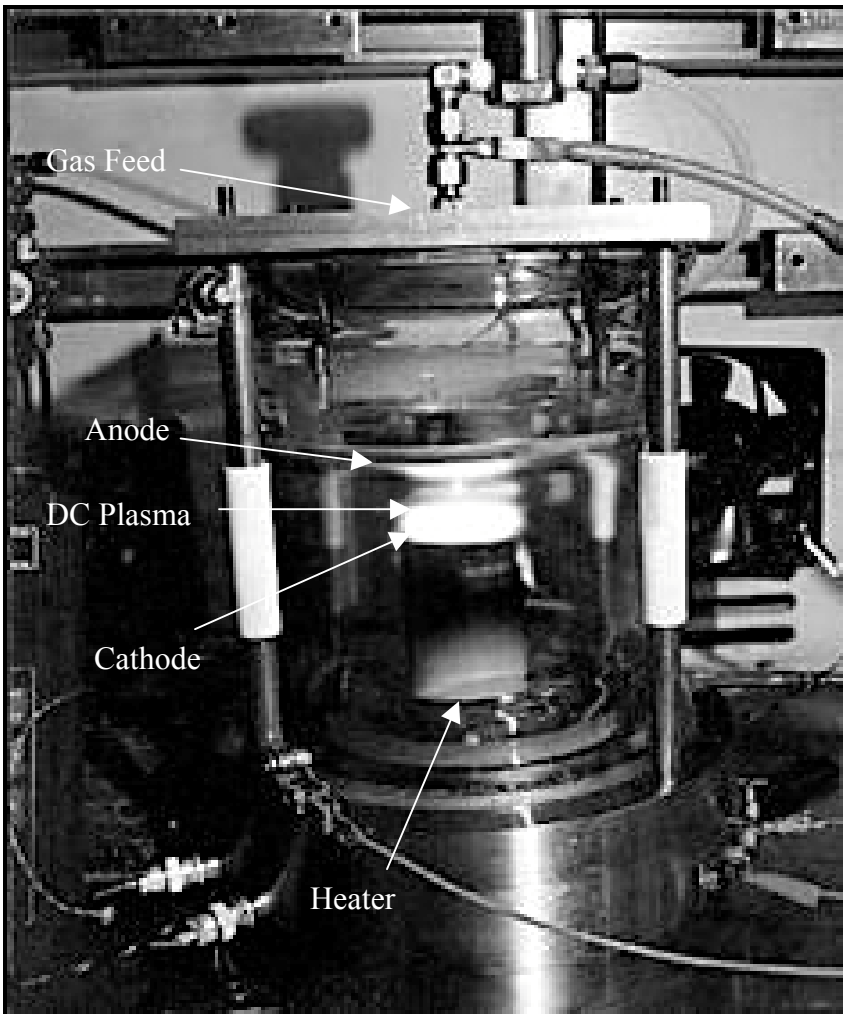


Figure 4.3 : PECVD nanofiber growth system.

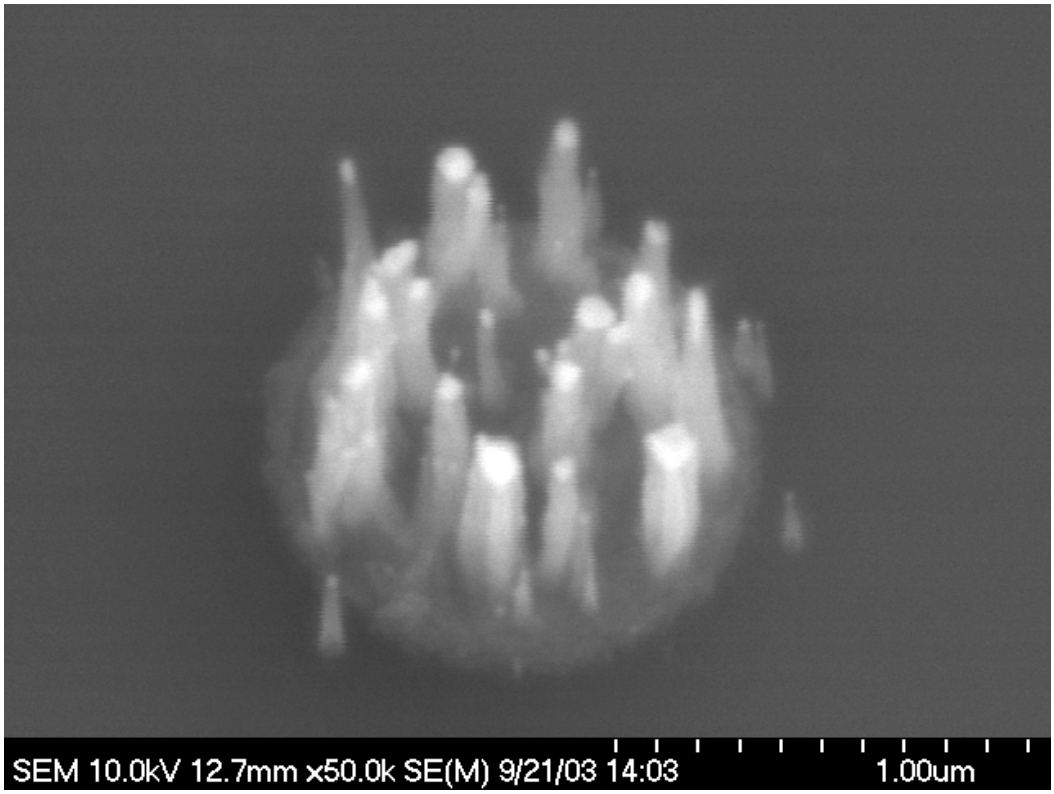


Figure 4.4: Carbon nanofiber cathode.

4.5 Chemical Mechanical Polishing

Because nanofibers were grown before the oxide deposition, the surface of the oxide required planarization before depositing a gate metal[4.3]. The chemical mechanical polishing (CMP) step removes bulges in the oxide above the nanofibers. A Strasbaugh 6EC CMP tool was used for this process. Before polishing, oxide was deposited at least 1.5 μm more than the desired thickness, as the CMP process removes oxide as it polishes. The polishing process was stopped before the oxide thickness was polished down to 0.5 μm above the nanofibers to protect them from damaged. The oxide removal rate varied between 150 and 450 nm/min.

4.6 Integration of Carbon Nanotubes with Microfabricated Structures

The complete fabrication process for carbon nanotube gated cathode devices is shown below in Figure 4.5 (see section 4.8 for the triode fabrication process). Figure 4.5(a) represents the catalyst lithography and deposition of 10 nm Al and 1 nm Fe. PECVD deposition of the oxide insulator is shown in Fig. 4.5(b) followed by the 50 nm Mo evaporation to form the gate (Fig. 4.5(c)). Figure 4.5(d,e) represent the photolithographic patterning of the gate aperture and aperture etch using RIE. The TCVD growth of carbon nanotubes is the final fabrication step (Fig. 4.5(f)).

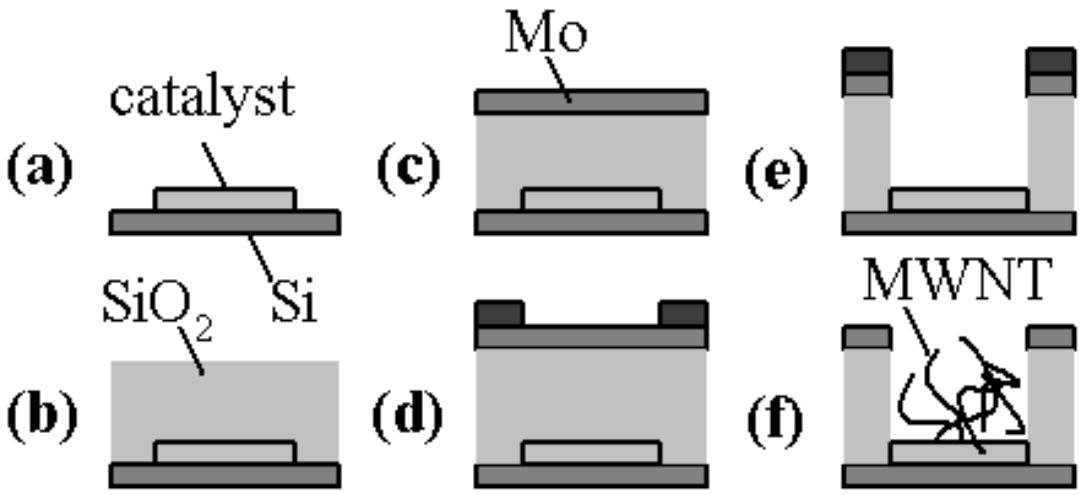


Fig 4.5: Carbon nanotube gated cathode device fabrication process.

One of the difficulties faced when trying to integrate carbon nanotubes into the field emission devices is controlling the size, length, and density of the nanotubes. This problem is enhanced by a variation in catalyst properties across a wafer and also from wafer to wafer. As mentioned in section 4.2, the oxide thickness deposited over the catalyst metal is somewhat non-uniform across the wafer as is the etch rate during RIE. Because of these non-uniformities, catalyst sites are exposed to the oxide etching plasma for varying lengths of time.

Although the catalyst metal does not chemically interact with the active species of the plasma during the oxide etch, it can be physically sputtered by energetic ions from the plasma. An overetch can result in catalyst metal being sputtered onto the sidewalls of the device. Figure 4.6 shows the result of the nanotube growth on such a device. The

catalyst metal at the bottom of the well had been sputtered onto the sidewalls of the device, so that no nanotubes grew on the cathode. The existence of the nanotubes on the sidewall of the device is further evidence that a thin layer of catalyst material was sputtered there. Although the overetch depicted in Figure 4.6 is an extreme example and can be avoided, the exposure of the catalyst sites to the plasma for varying lengths of time can affect the reproducibility of the thermal CVD process.

One way of avoiding the exposure of catalyst sites to the plasma would be to etch the oxide in hydrogen fluoride rather than using the RIE, as is done with nanofiber devices. Unfortunately, the HF etches the aluminum and lifts off the iron, preventing nanotube growth.

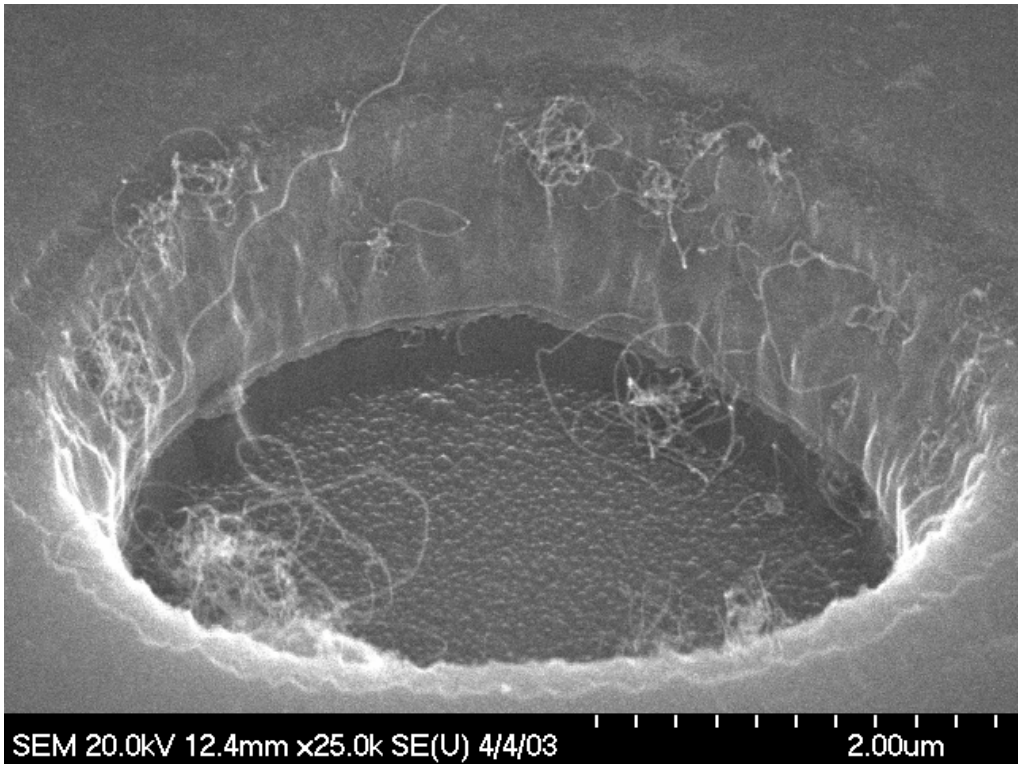


Figure 4.6: CVD result on an overetched gated cathode device.

A high density of nanotubes is desired to provide multiple emission sites on the cathode. The length of these nanotubes should be considerably less than the distance from the cathode to the gate electrode, so that nanotubes will not electrically connect the gate and cathode. Although the growth rate during TCVD is not linear, one way of controlling the length of the nanotubes is to vary the growth time. The growth rate can also be affected by varying the growth temperature and acetylene flow rate. However, a given growth process often will not produce the same results on different samples from the same wafer. For this reason, thin dense films of nanotubes are achievable, but difficult to repeat.

Another method of controlling the nanotube length is to etch a thick film of nanotubes back to a desired thickness in an oxygen plasma. Figure 4.7 below shows a device before and after etching for 30 seconds in an oxygen plasma. This device was tested and emitted with a turn on voltage of 40 volts.

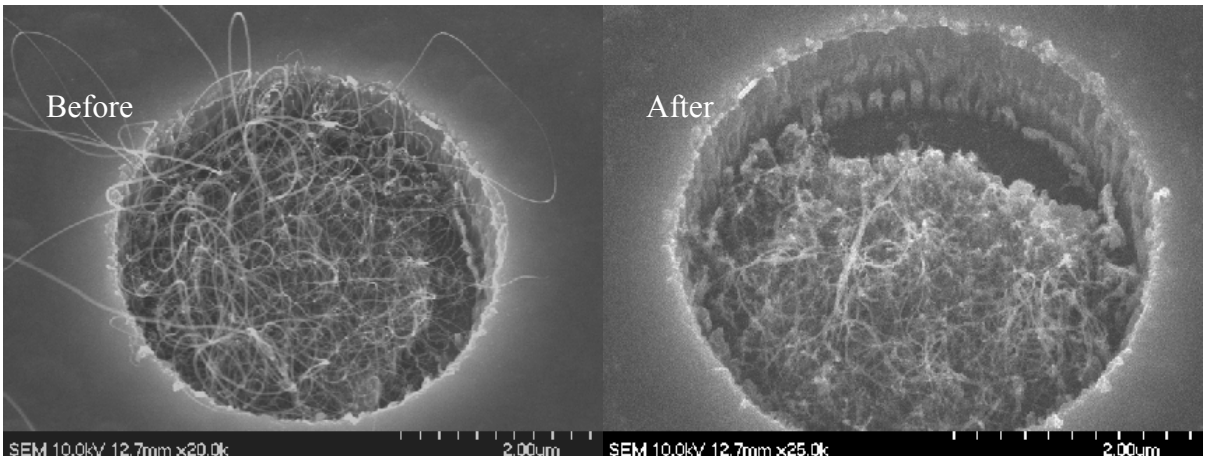


Figure 4.7: Etching of nanotubes in a 30 second oxygen plasma.

Another difficulty involved with growing carbon nanotubes in gated FE devices is the deposition of a thin carbon film on the surface of the sidewall of the device during TCVD growth. This film provides a path for leakage current between the cathode and gate, as is reported in chapter 5. To explore the cause of this film deposition, gated cathode devices without catalyst metal were subjected to the nanotube growth procedure. When a voltage was applied between the cathode and gate, no gate leakage current occurred. In this way it was determined that the acetylene gas (C_2H_2) did not deposit a carbon film on the sidewall of the device, but it did react with the catalyst site to form a product that deposits on the sidewall of the devices. It was found that devices with the smaller catalyst sites (formed using the step and repeat photolithography system) did not have significantly less gate leakage current than those with large catalyst sites. The leakage current was the main reason for the decision to experiment with the fabrication of carbon nanofiber FE devices. Since the nanofibers are grown before the oxide is deposited, there is no carbon film deposited onto the sidewall.

4.7 Integrating Carbon Nanofibers into Field Emission Devices

The fabrication process for multiple carbon nanofiber gated cathode devices is shown below in Figure 4.8. After the catalyst site was patterned and metal deposited (Fig. 4.8(a)), the PECVD nanofiber growth process was performed (Fig. 4.8(b)). Next the SiO_2 was deposited (Fig. 4.8(c)) and the surface was planarized using the CMP tool (Fig. 4.8(d)). The gate metal was then deposited (Fig. 4.8(e)) using electron gun PVD. Finally, the gate aperture was photolithographically defined. The photoresist served as an

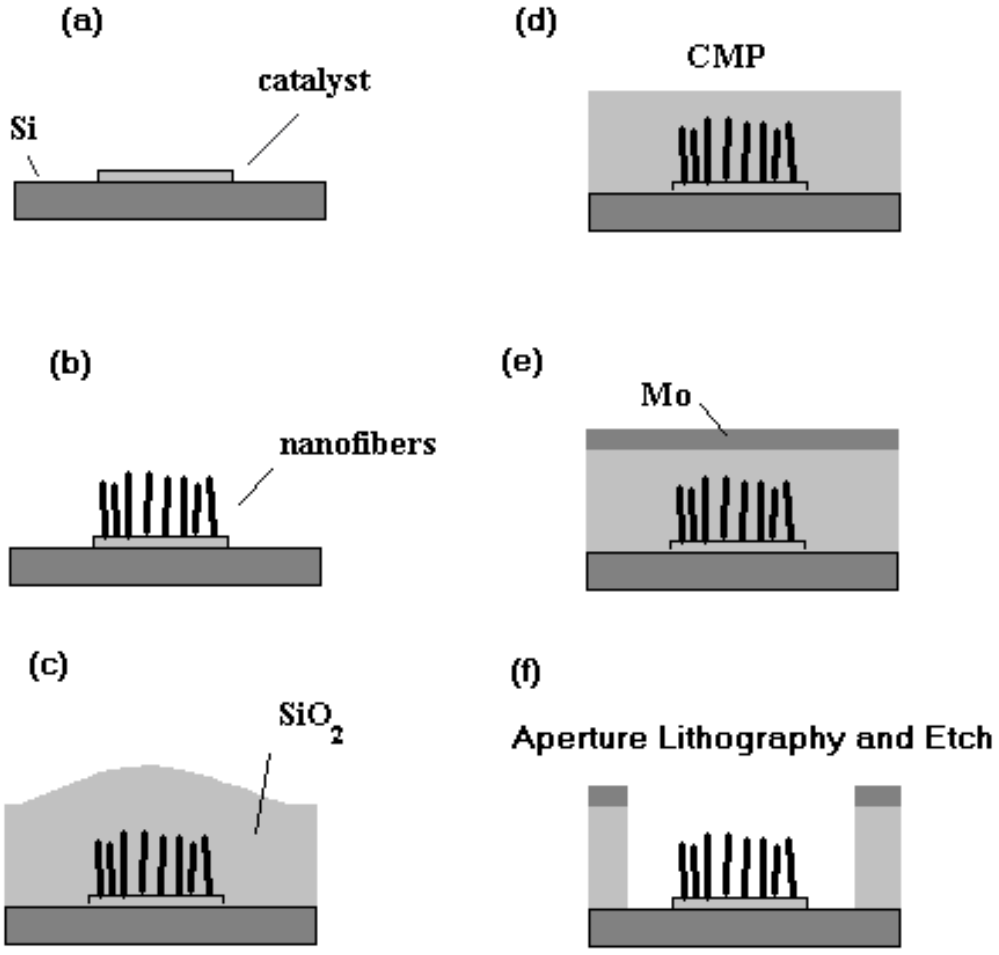


Figure 4.8: Carbon nanofiber gated cathode fabrication process.

etch mask during the RIE through the gate metal. The device was completed with an HF etch through the oxide (Fig. 4.8(f)) and a resist strip.

The carbon nanofiber growth process proved to be more repeatable and controllable than the CVD growth process for nanotubes, but there are many issues that are involved with incorporating nanofibers into FE devices. Perhaps most importantly, nanofibers grown under certain conditions will not survive an oxide deposition followed by an HF dip, as shown in Figure 4.9 below.

The nanofibers in Fig. 4.9 were grown using the process described in section 4.4 with the exception of the acetylene flow, which was ramped from 20 to 56 sccm during the first minute of growth. The bases of the nanofibers are oxidized during the oxide deposition and removed from the substrate by the HF oxide etch.

Fortunately, some nanofibers grown in a lower acetylene flow rate (50 sccm) survived the oxide deposition and removal. These fibers have a protective sheath of

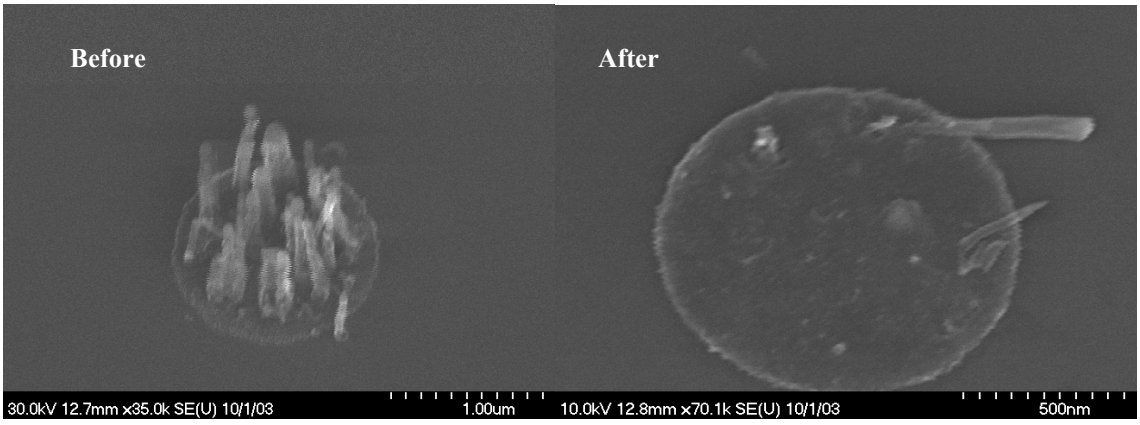


Figure 4.9: Carbon nanofibers before and after oxide deposition and removal.

silicon that is sputtered from the substrate onto their sides during the growth. The outer layer of silicon in this sheath is oxidized during the oxide deposition, but the base of the nanofiber is protected. A decrease in diameter at the base of the nanofibers occurs because part of the sheath is removed (see Figure 4.10 below). Unfortunately, only the larger nanofibers with more sheath material survive the oxide deposition and etch, and these fibers have large tips compared to nanofibers grown at higher acetylene flow rates. The larger tips increase the threshold for field emission.

The difficulty of fabricating carbon nanofiber FE devices is increased with the addition of the CMP step (which is not required for fabricating nanotube devices). The problems faced with the oxide deposition, CMP, and HF etch would be avoided if nanofibers were grown in a microfabricated well after the insulator and gate were in place. Unfortunately, the PECVD fiber growth process damages the gate electrodes[4.4].

The complete fabrication of a multiple carbon nanofiber gate cathode was not

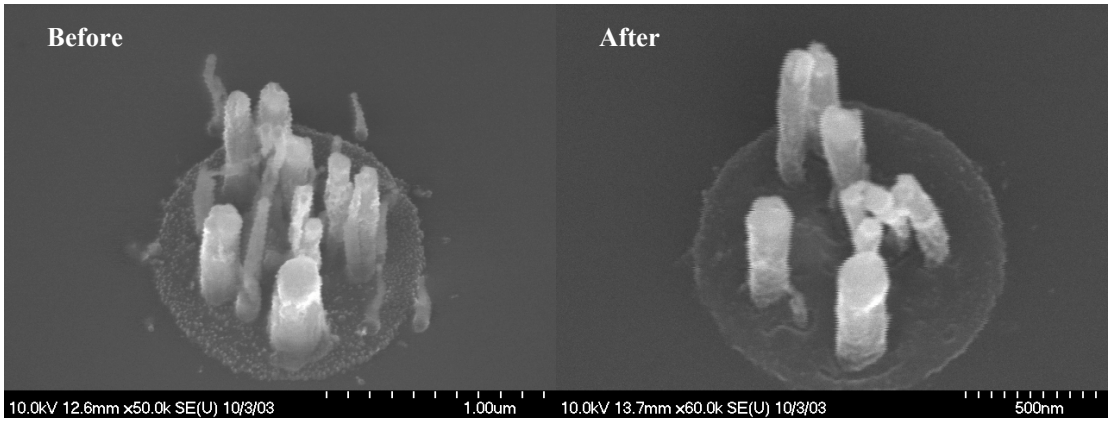


Figure 4.10: Carbon nanofibers grown at 50 sccm C_2H_2 before and after oxide deposition and removal.

achieved for this work. This type of device would have the advantage of less gate current over the multiwall nanotube devices, but an important disadvantage of higher field emission threshold due to the larger tips.

4.8 Fabrication of Carbon Nanotube Triode Devices

Carbon nanotube FE devices with a second gate were achieved using the fabrication process shown in Figure 4.11. The steps shown in Fig. 4.11 (a)-(c) are the same initial steps for gated cathode device fabrication (also shown in Fig.4.5 (a)-(c)). After the first gate electrode deposition, another layer of SiO_2 dielectric was deposited (Fig. 4.11 (d)) and the second gate electrode was deposited (Fig. 4.11 (e)). To contact the first gate electrodes, vias above the contact pads were photolithographically defined. The oxide was removed from the pads with a plasma etch. These steps are depicted in Figure 4.11 (f) and (g). Next the gate aperture photolithography was performed, followed by reactive ion etching through the oxide and gate layers to expose the catalyst site (Fig. 4.11 (h,i)). Finally, the TCVD growth process for carbon nanotubes was performed (Fig. 4.11 (j)). Field emission data from these devices can be found in chapter 5.

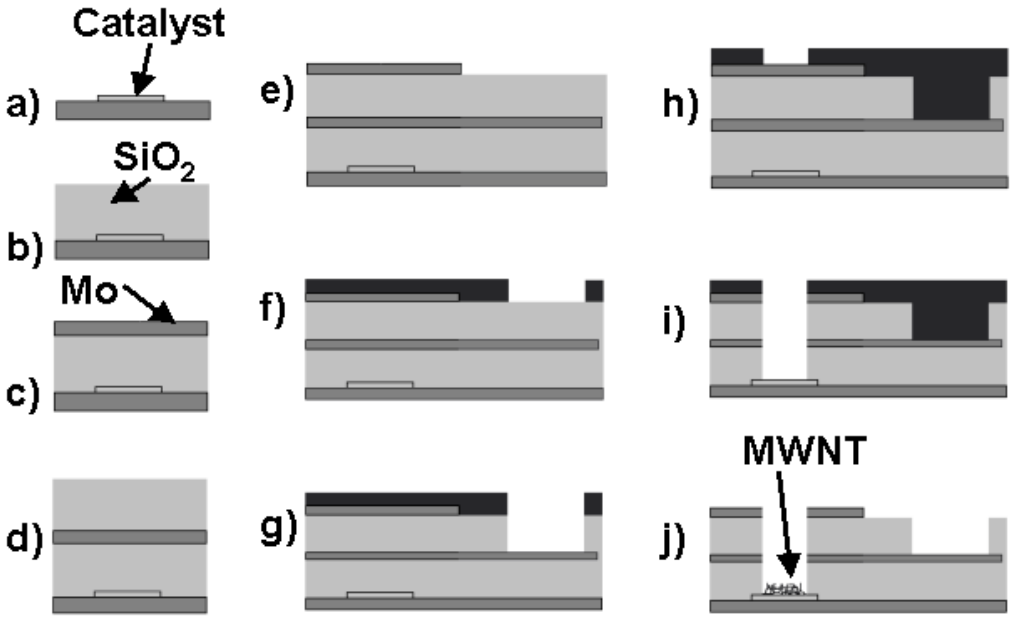


Fig. 4.11: Fabrication process for multiwall carbon nanotube triode devices.

Chapter 5

Experimental Procedures and Results

5.1 Experimental Setup and Procedure

The field emission devices fabricated for this work are not vacuum sealed, so testing was performed in a vacuum chamber evacuated by roughing and turbomolecular pumps. Testing was done at pressures of less than 6 E-6 Torr. After dicing the wafer, the chips were placed on a chip board. Electrons emitted from the cathode were collected by a copper anode placed 1mm above the chip. Conductive carbon tape was used to hold the chip in place and to connect the substrate of the chip to the ground plane of the chip board. The chip board was placed on the copper test board shown below in Figure 5.1.

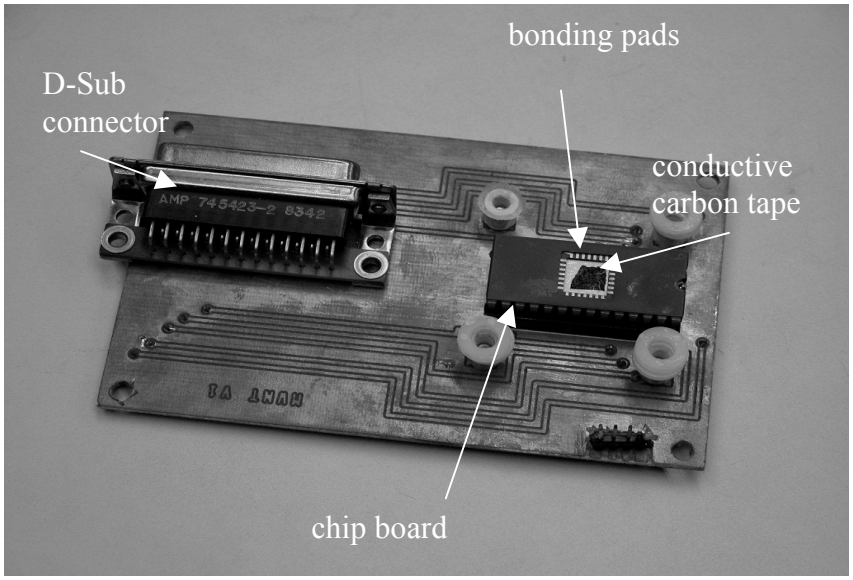


Figure 5.1: Test board for DC measurements.

Each gate electrode was bonded to the chip board's pads using an aluminum wedge wire bonder. A 25-pin D-Sub cable connected the test board to a switch box outside of the vacuum chamber. The anode connection was wired to a separate feedthrough on the vacuum chamber. The switchbox has 21 3-way switches that were used to test devices operating individually or in an array. The switchbox is shown in Figure 5.2.

The gate, cathode, and anode voltages were controlled by Keithley Instruments model 2410 source measurement units (SMU), which were controlled by a Keithley 2367 trigger controller. ICS measurement software was used to program the SMUs and capture data. Figure 5.3 shows a diagram of the measurement setup.

5.2 Experimental Results from Carbon Nanotube Gated Cathode FE Devices

During testing, the anode was biased at 100V, the gate electrodes were grounded, and the cathode was swept from 0 to –100V. Before obtaining FE I-V curves, a voltage sweep was performed to blow out any nanotubes providing a short between the gate electrodes and the cathode. The I-V curve in Figure 5.4 shows a sudden drop in the cathode current as the short producing nanotubes are blown out. Immediately following the drop in cathode current, a sudden increase in emission current to the anode was observed due to the increase in the electric field at the cathode after the short circuits were removed.

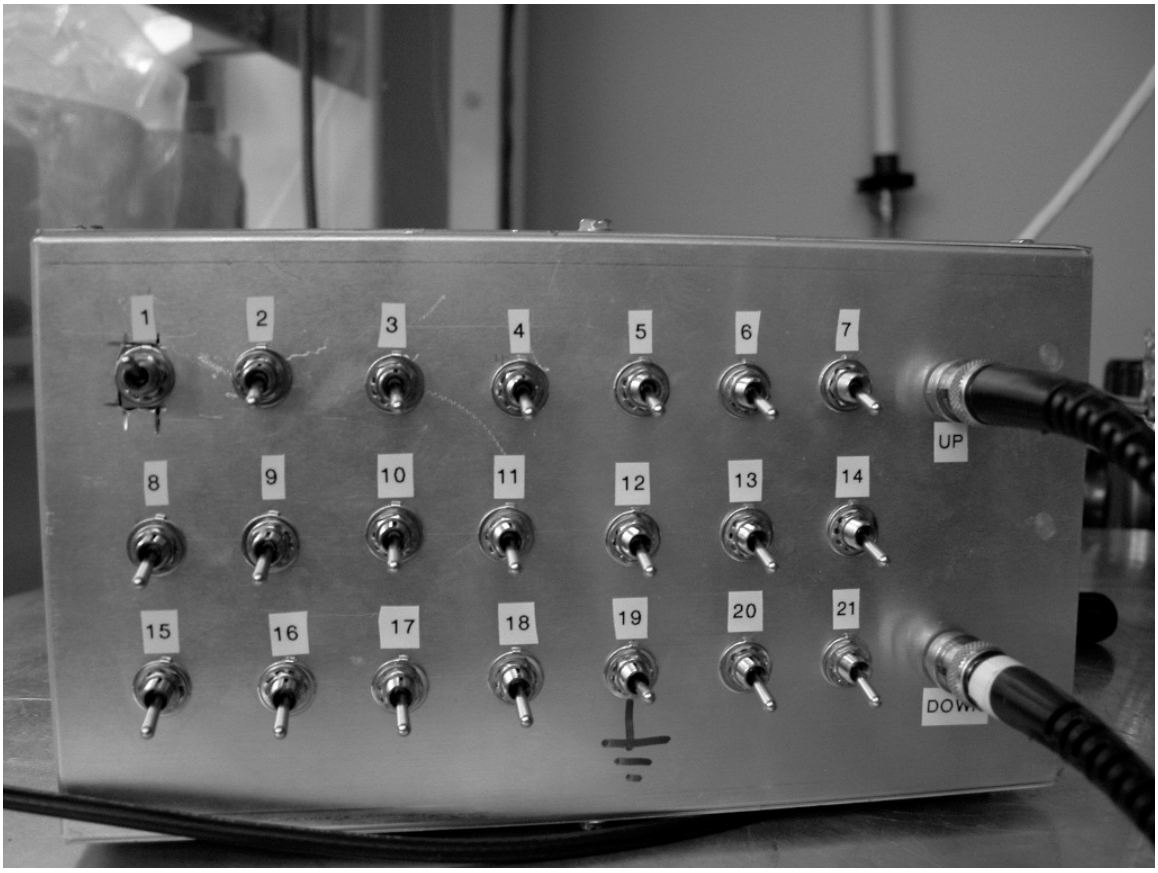


Figure 5.2: Switchbox for DC testing of FE devices.

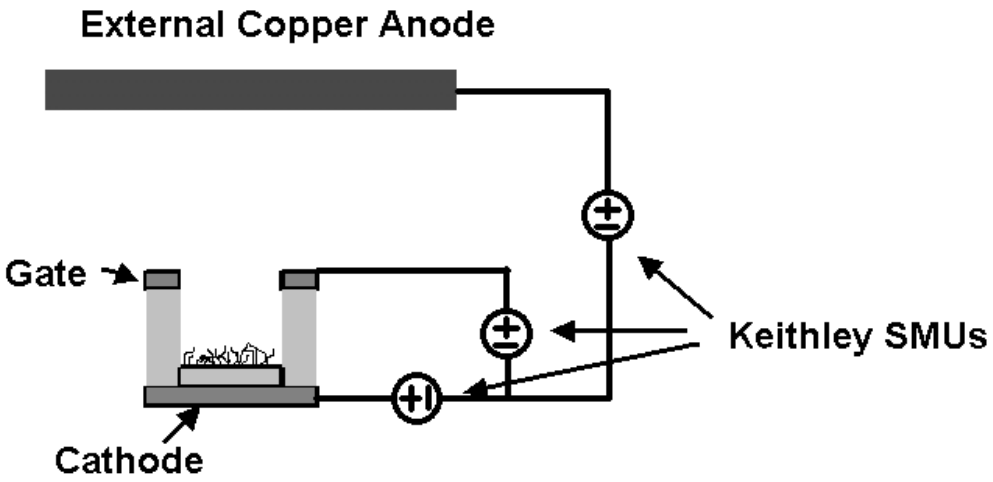


Figure 5.3: Measurement setup.

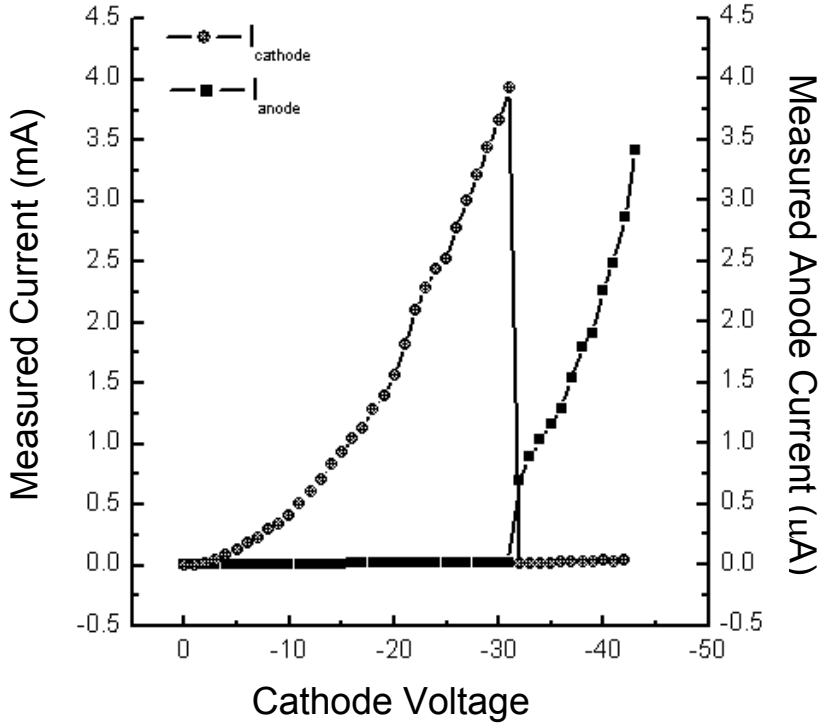


Figure 5.4: A blowout curve performed prior to FE testing.

After obtaining the blowout curve, the FE devices were tested as an array. Figure 5.5 shows the FE I-V curve from an array of 9 gated cathode devices and shows a threshold voltage of ~22V. The threshold voltage was defined as the voltage between the gate and cathode required to generate 10 nA of current from the array of devices. For individual devices, threshold voltages were defined as the voltage required to generate 1 nA of current from the cathode. The anode current from this array was plotted in Fowler-Nordheim coordinates (Figure 5.6) and was found to be linear, indicating that the emission was occurring through the tunneling process described in Chapter 3.

The I-V characteristics from two different individual field emitters are shown in Figures 5.7 and 5.8. For these curves, the gates of all the other devices in the array were connected to the cathode voltage. These two devices have threshold voltages of 25 and 50 V. The Fowler-Nordheim plot of the first device (Inset of Figure 5.7) has two different distinct regions whose linear fits have different slopes. This could indicate that the behavior of the emission site changed during the voltage sweep, or may represent two different emission sites within the device. Some noise in these emission curves may be due to multiple emission sites.

To test the change in emission characteristics with time, devices were tested with a constant voltage between the gate and cathode. Figure 5.9 shows the operation of an individual FE device before and after 40 minutes of operation with a constant cathode voltage of –30 V. These curves show that the threshold voltage of the device decreased from 34 to 22 V during the constant bias operation. There was also an increase in noise after the period of constant bias operation.

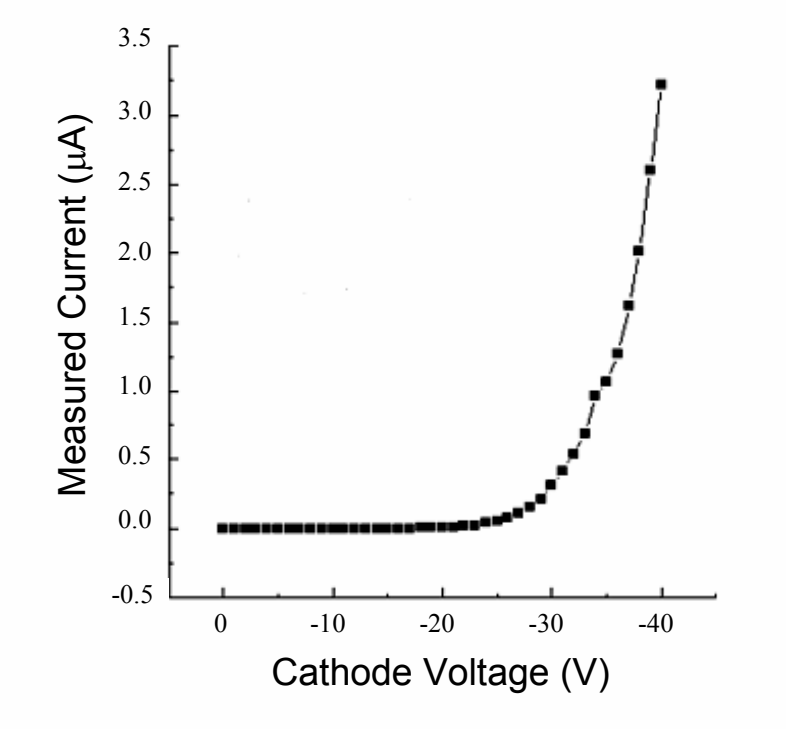


Figure 5.5: FE I-V curve from an array of FE devices.

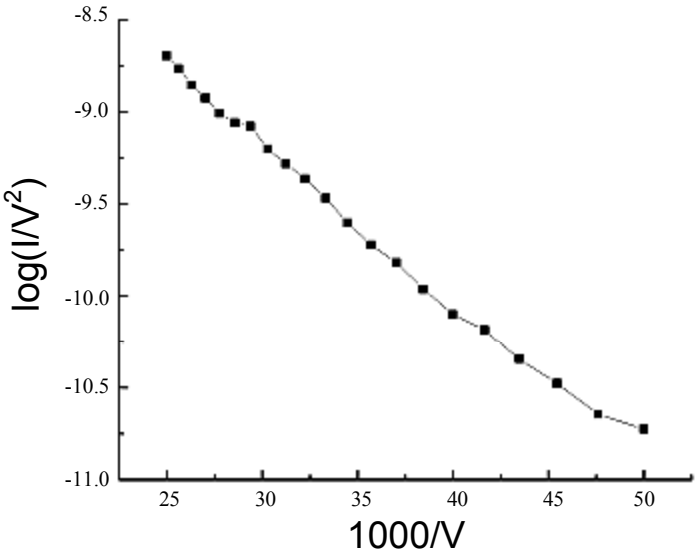


Figure 5.6: Fowler-Nordheim plot of anode current.

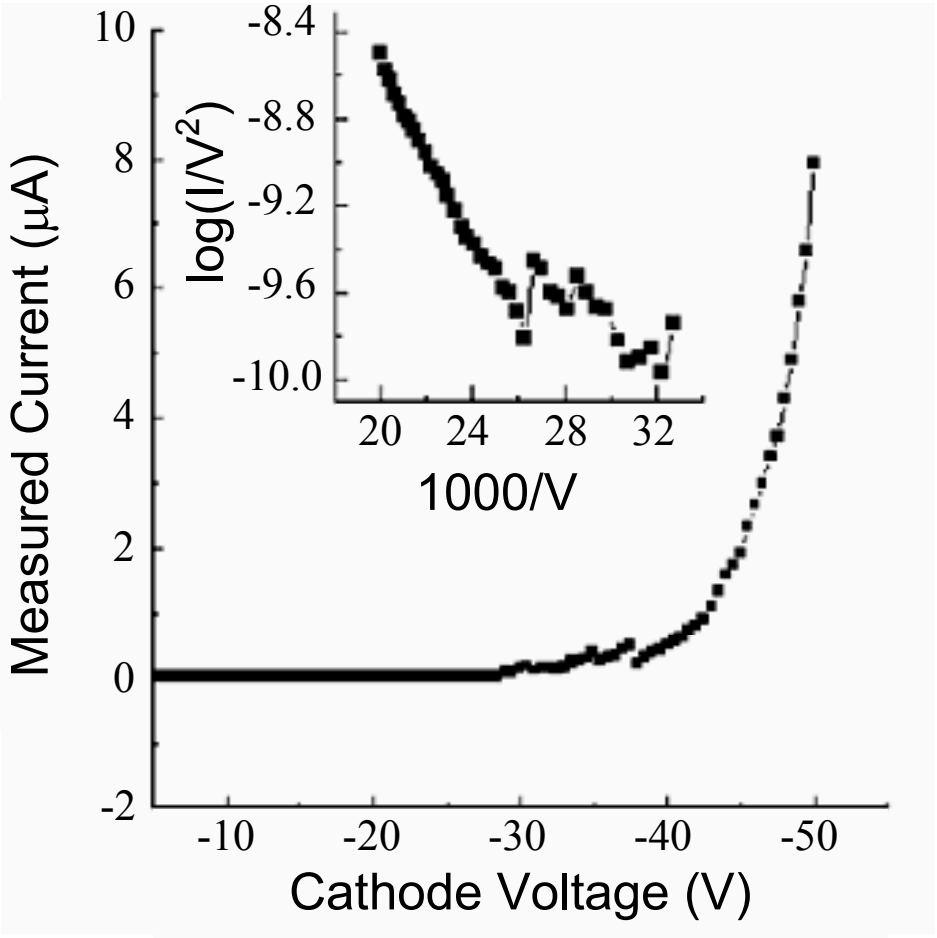


Figure 5.7: Field emission from an individual device. Inset: Data in F-N coordinates.

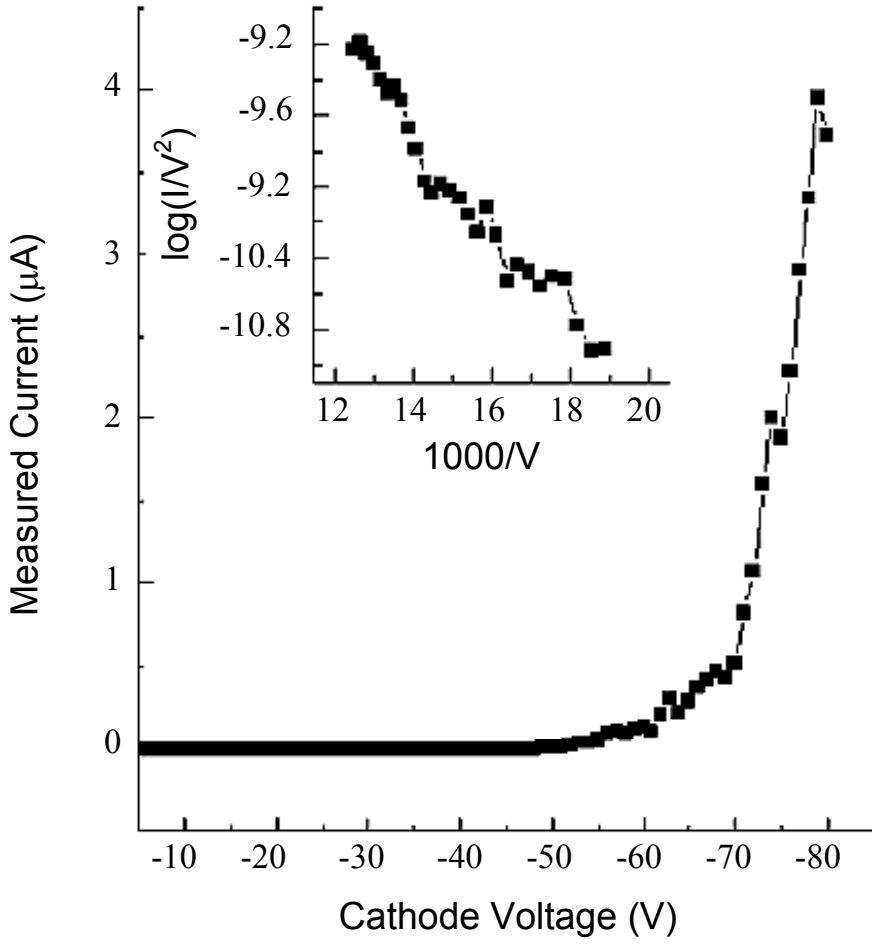


Figure 5.8: Field emission from an individual gated cathode device. Inset: Data plotted in Fowler-Nordheim coordinates.

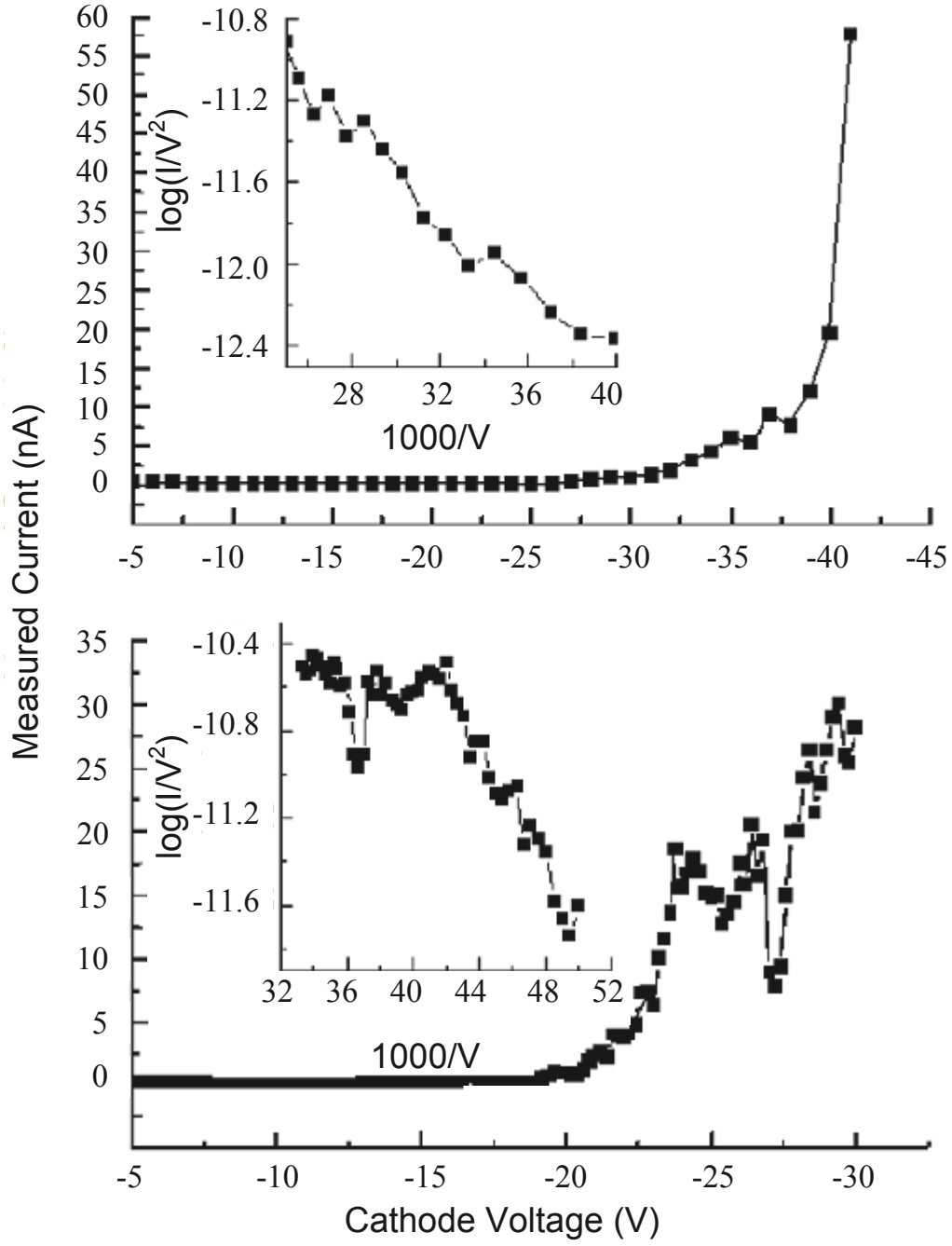


Figure 5.9: Top: Emission before 40 minutes of constant voltage bias. Bottom: Emission after constant bias operation.

5.3 Experimental Results from Carbon Nanotube Triode FE Devices

The triode devices were tested using the same experimental setup as was used for the gated cathode devices. The second electrode was used as a stacked gate to enhance emission rather than to collect current. A copper anode was spaced above the chip to collect current as with the gated cathode devices. An SEM image of a carbon nanotube triode device is shown below in Figure 5.10.

The triode devices were tested with an anode voltage of 500 V. The cathode voltage was kept grounded while either the first or second gate voltage was swept. Figure 5.11 below shows the operation of an array of triode devices with the 2^{nd} gate voltage kept constant while sweeping the lower gate voltage from 0 to 60 V. The 2^{nd} gate initiated emission at 60 V with the 1^{st} gate grounded. Figure 5.12 shows the triode operating with constant voltages at the 1^{st} gate and a swept voltage on the 2^{nd} gate. The I-V relationship in Figure 5.12 appears more linear than exponential. From this it can be concluded that the affect of the 2^{nd} gate voltage on the cathode field is not linear. These curves demonstrate that the 2^{nd} gate is affecting the emission current. If the 2^{nd} gate were encapsulated, it could be biased below its threshold voltage for use as an anode in a sealed triode device.

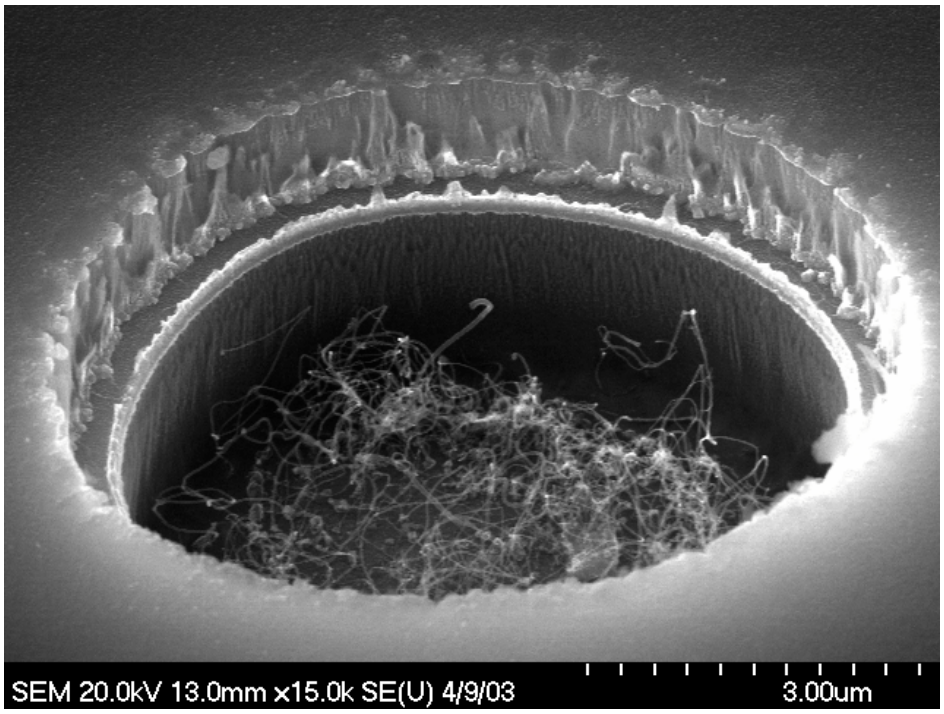


Figure 5.10: Carbon nanotube triode FE device.

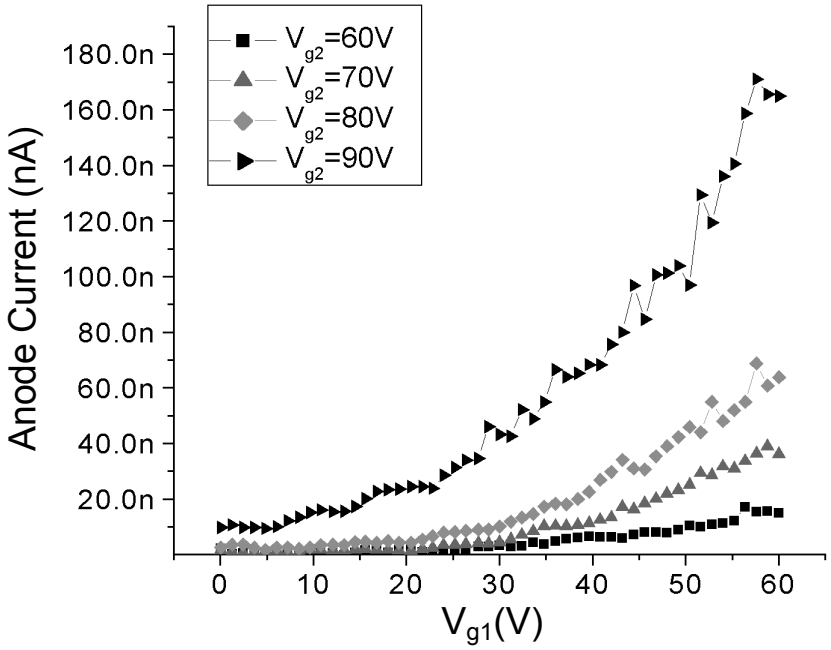


Figure 5.11: Carbon nanotube triode operation with constant 2nd gate voltage.

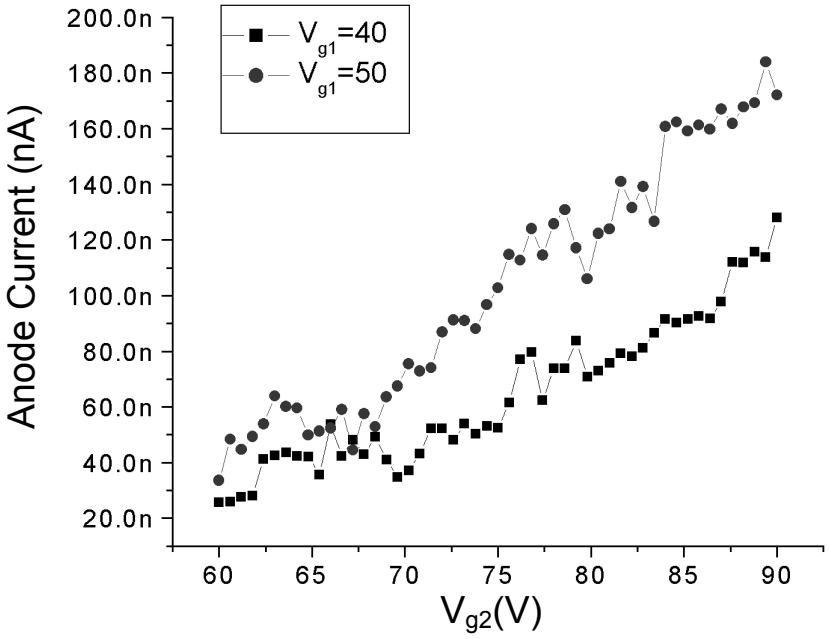


Figure 5.12: Carbon nanotube triode operation with constant 1st gate voltage.

5.4 Drawbacks of the Electrical Characteristics of Carbon Nanotube Gated Cathodes and Triodes

One limitation of the carbon nanotube FE devices is the stability of the emission current. The current stability could be improved by using a resistance in series with the cathode of the device, causing a decrease in the voltage between the gate and cathode as the emission current increases. The main problem with the electrical characteristics of these devices is the leakage current between the cathode and the gate voltage, which is caused by the thin carbon film on the sidewall of the device. Most devices tested (that successfully emitted) received less than 10 % of cathode current to the anode. While

some of the emitted electrons are collected by gate electrodes, the gate current is mainly due to leakage. This was verified by sweeping the gate voltage from a negative potential to a positive one. The existence of gate current at potentials below the cathode can not be due to emission. The magnitude of the cathode current is higher for a positive gate voltage, indicating that both leakage current and emission current is occuring.

Chapter 6

Conclusion

6.1 Summary and Analysis of Carbon Nanotube Field Emission Devices

The results from carbon nanotube FE devices in the previous chapter show that these devices need many improvements to be competitive with solid state devices. The gate leakage current of these devices must be significantly decreased. Attempts in this work at removing the carbon sidewall film in these devices by plasma and wet etching were unsuccessful. An important advantage of carbon nanofiber FE devices over nanotube devices is the lack of this carbon film.

More work needs to be done on developing methods of consistently growing nanotubes with desirable properties. Vacuum sealing of these devices is also needed so that they can be operated outside of vacuum chambers.

6.2 Summary and Analysis of Carbon Nanofiber Field Emission Devices

Unfortunately, current-voltage data for multiple VACNF FE devices was not obtained in this work. If the fabrication difficulties discussed in section 4.7 are overcome in the future, a VACNF FE device will likely offer significant advantages over the MWNT devices measured in this work. Since the nanofibers are grown before the oxide is deposited, there should be no carbon film on the sidewall of the device to allow gate

leakage current. Controlling the growth process proved to be less difficult for nanofibers than nanotubes. Unless improvements are made in controlling nanotube growth, mass production of a FE device that requires precise control of the emitter characteristics seems more feasible using nanofibers than nanotubes.

A disadvantage of the nanofibers grown for this work is that they have larger tips than the nanotubes. The larger tips will increase the turn-on voltage required for emission. The turn-on voltage for the FE devices can be decreased if the gate electrodes are closer to the cathode and the gate aperture is decreased. More precision in the fabrication process is needed for this improvement.

If the obstacles mentioned above are overcome, carbon nanotube and nanofiber FE devices will be promising candidates for high temperature and high frequency applications.

References

References

Chapter 1:

1.1. I. Brodie, P.R. Schwoebel, Proceedings of the IEEE 82 (1994).

1.2. K.R. Shoulders, Adv. Computers 2 (1961).

1.3. D. Temple, Materials Science and Engineering, R24 (1999).

1.4. C. Bower, et al., IEEE Transactions on Electron Devices, Vol. 49, No. 8, (2002).

1.5. C. A. Spindt, J. Appl. Phys. 39 (1968).

1.6. D. Hsu and J. Shaw, Appl. Phys. Lett. 80, 118 (2002).

1.7. K. Park et al., J. Vac. Sci. Technol. B 21(4), (2003).

1.8. K. A. Dean and B. R. Chalamala, Appl. Phys. Lett. 75, 3017 (1999).

1.9. X. Xu and G.R. Brandes, Mater. Res. Soc. Symp. Proc. 509, 107 (1998).

1.10. H-C Cheng et al, Electrochemical and Solid-State Letters, 4 (2001).

1.11. M. A. Guillorn, M.D. Hale, V.I. Merkulov, M.L. Simpson, G.Y. Eres, H. Cui, A.A. Puretzky, and D.B. Geohegan, J. Vac. Sci. Technol. B 21(3), (2003).

1.12. Q. H. Wang, M. Yan, and R.P.H. Chang, Appl. Phys. Lett. 78, 1294 (2001).

1.13. C. Bower, W. Zhu, et al., Appl. Phys. Lett. 80, 3820 (2002).

1.14. M.A. Guillorn, M.L. Simpson, G.J. Bordonaro, V.I. Merkulov, L.R. Baylor, and D.H. Lowndes, J. Vac. Sci. Technol. B 19, 573 (2001).

Chapter 2:

2.1. Richard L. C. Wu, A. K. Rai, A. Garscadden, P. Kee, H. D. Desai, K. Miyoshi, J. Appl. Phys. 72 No. 1 (1992).

2.2. D. M. Gruen, Annu. Rev. Mater. Sci. **29**, 211 (1999).

2.3. J. Philip, P. Hess, T. Feygelson, J. E. Butler, S. Chattopadhyay, K. H. Chen, L. C. Chen, J. Appl. Phys. 93 No. 4 (2003).

2.4. W. P. Kang, J. L. Davidson, A. Wisitsora-at, M. Howell, A. Jamaludin, Y. M. Wong, K. L. Soh, D. V. Kerns, J. Vac. Sci. Technol. B 21 No. 1 (2003).

2.5. H. K. Woo, S. T. Lee, C. S. Lee, I. Bello, Y. W. Lam, J. Vac. Sci. Technol. A 15 No. 6 (1997).

2.6. H. W. Kroto, J. R. Heath, S. C. O'Brien, R. F. Curl, R. E. Smalley, Nature 318 (1985).

2.7. Andrzej Huczko, Przemysław Byszewski, Fullerenes and Carbon Nanotubes, 1998, 5.

2.8. O. E. Andersson, B. L. V. Prasad, H. Sato, T. Enoki, Y. Hishiyama, Y. Kaburagi, M. Yoshikawa, and S. Bandow, Phys. Rev. B 58, (1998).

2.9. Min Ouyang, Jin-Lin Huang, and Charles M. Lieber, Annu. Rev. Phys. Chem. 53, (2002).

2.10. Jean-Marc Bonard , Christian Klinke, Kenneth A. Dean, and Bernard F. Coll, Phys. Rev. B 67, (2003).

2.11. V. I .Merkulov, D. H. Lowndes, Y. Y. Wei, G. Eres, and E. Voelkl, Appl. Phys. Lett. 76 (2000).

2.12. Z. F. Ren, Z. P. Huang, D. Z. Wang, J. G. Wen, J. W. Xu, J. H. Wang, L. E. Calvet, J. Chen, J. F. Klemic, and M. A. Reed, Appl. Phys. Lett. 75 (1999).

2.13. L. R. Baylor, D. H. Lowndes, M. L. Simpson, C. E. Thomas, M. A. Guillorn, V. I. Merkulov, J. H. Whealton, E. D. Ellis, D. K. Hensley, and A. V. Melechko, J. Vac. Sci. Technol. B 20(6) (2002).

2.14. M. A. Guillorn, T. E. McKnight, A. Melechko, V. I. Merkulov, P. F. Britt,

D. W. Austin, D. H. Lowndes, and M. L. Simpson, J. Appl. Phys. 91, (2002).

2.15. A. V. Melechko, T. E. McKnight, M. A. Guillorn, V. I. Merkulov, B. Ilic, M. J. Doktycz, D. H. Lowndes, and M. L. Simpson, Appl. Phys. Lett. 82 (2003).

Chapter 3:

3.1. D. Temple, Materials Science and Engineering, R24 (1999).

3.2. R. H. Fowler, L. Nordheim, Proc. of the Royal Society of London. Series A, Vol. 119, No. 781 (May 1 1928), 173-181.

3.3. Millikan and Eyring, 'Phys. Rev.,' vol. 27, p. 51 (1926).

3.4. P. Chen, X. Wu, X. Sun, J. Lin, W. Ji, and K. L. Tan, Phys. Rev. Lett. **8**2, 1999.

3.5. H. Ago, T. Kugler, F. Cacialli, W. R. Salaneck, M. S. P. Shaffer, A. H. Windle, and R. H. Friend, J. Phys. Chem. B 103, 1999.

3.6. C. Dong, M. Gupta, Appl. Phys. Lett., Vol. 83, No. 1, 2003

3.7. B. Chalamala, R.M. Wallace, B.E. Gnade, Proc. 43rd National Symposium of the American Vacuum Society, Philadelphia, PA, 1996, p.141.

3.8. C.A. Spindt, C.E. Holland, A. Rosengreen, I. Brodie, Electron Devices Meeting, 1993. Technical Digest., International, p. 749-752.

3.9. C. A. Spindt, C. E. Holland, P. R. Schwoebel, I. Brodie, Vacuum Microelectronics Conference, 1995. IVMC., 1995 International, p. 137.

3.10. K. Dean, T. Burgin, B. Chalamala, Appl. Phys. Lett., Vol. 79, No. 12, 2001.

3.11. J. Bonard C. Klinke, K. Dean, B. Coll., Phys. Rev. B. 67 (2003).

Chapter 4:

4.1. M. A. Guillorn, M.D. Hale, V.I. Merkulov, M.L. Simpson, G.Y. Eres, H. Cui, A.A. Puretzky, and D.B. Geohegan, J. Vac. Sci. Technol. B 21(3), (2003).

4.2. M.A. Guillorn, M.L. Simpson, G.J. Bordonaro, V.I. Merkulov, L.R. Baylor, and D.H. Lowndes, J. Vac. Sci. Technol. B 19, 573 (2001).

4.3. M. A. Guillorn, A. V. Melechko, V. I. Merkulov, D. K. Hensley, M. L. Simpson, and D. H. Lowndes, Appl. Phys. Lett. 81, (2002).

4.4. M. A. Guillorn, 2003. [dissertation]. University of Tennessee: Knoxville (TN). Available from: University of Tennessee.

Vita

Mark Hale was born in Kingsport, Tennessee on March 24, 1980. He graduated from Sullivan Central High School in 1998. Mark entered the University of Tennessee in the fall of 1998 to pursue an undergraduate degree in Electrical Engineering. He received the UT Valedictorian and Bicentennial scholarships. The main focus of his studies as an undergraduate was in electronic devices and circuit design. Mark worked as a summer intern in the Display Electronics Product Laboratory at Analog Devices Inc. during his undergraduate studies. During the last semester of his undergraduate studies, Mark began work as an undergraduate research assistant in the Molecular-scale Engineering and Nanoscale Technologies (MENT) research group at Oak Ridge National Laboratory. He graduated in the spring of 2002 with a Bachelor of Science in Electrical Engineering, *Summa cum Laude*.

After graduating, Mark continued work at ORNL as a graduate research assistant while continuing his studies and pursuing a Master of Science degree at the University of Tennessee. Mark studied under the direction of Professor Michael L. Simpson, the Principle Investigator of the MENT group. Mark was awarded the Robert E. Bodenheimer Fellowship during his graduate studies.

After completing his Master's degree Mark will study in pursuit of the Ph. D. in Electrical Engineering under the direction of Professor Benjamin J. Blalock. Mark's professional interests include analog circuit design, microelectronic device physics and fabrication, and vacuum nanoelectronics.